ORNL/TM-2023/2889

Research Plan and Preliminary Results in Developing the Fabrication Parameters for Alloy 709 in Different Product Forms —Grain Coarsening Temperature Evaluation

Yanli Wang
M. Grace Burke
Marcos K. M. Moritugui
Pedro de Souza Ciacco
Artur Pinto Ferreira
Mauricio C. V. Munoz
C. Isaac Garcia

April 2023

OAK RIDGE National Laboratory

ORNL IS MANAGED BY UT-BATTELLE LLC FOR THE US DEPARTMENT OF ENERGY

ORNL/TM-2023/2889

Materials Science and Technology Division

RESEARCH PLAN AND PRELIMINARY RESULTS IN DEVELOPING THE FABRICATION PARAMETERS FOR ALLOY 709 IN DIFFERENT PRODUCT FORMS —GRAIN COARSENING TEMPERATURE EVALUATION

Yanli Wang,
M. Grace Burke*
Marcos K. M. Moritugui†, Mauricio C. V. Munoz†, Pedro de Souza Ciacco†, Artur Pinto Ferreira†,
C. Isaac Garcia†

*Idaho National Laboratory
†University of Pittsburgh

April 2023

Prepared by
OAK RIDGE NATIONAL LABORATORY
Oak Ridge, TN 37831
managed by
UT-BATTELLE LLC
for the
US DEPARTMENT OF ENERGY
under contract DE-AC05-00OR22725

This page intentionally left blank.

CONTENTS

LIST OF FIGURES

LIST OF TABLES

ACKNOWLEDGMENTS

This research was sponsored by the US Department of Energy (DOE) under Contract No. DE-AC05-00OR22725 with Oak Ridge National Laboratory (ORNL), which is managed and operated by UT-Battelle LLC, and under Contract No. DE-AC07-05ID14517 with Idaho National Laboratory (INL), which is managed and operated by Battelle Energy Alliance. Programmatic direction was provided by the Office of Nuclear Reactor Deployment of the DOE Office of Nuclear Energy (NE).

The authors gratefully acknowledge the support provided by Sue Lesica of DOE-NE , Federal Materials Lead for the Advanced Reactor Technologies (ART) Program; Kaatrin Abbott of DOE-NE, Federal Manager, ART Fast Reactor Program (FRP); Bo Feng of Argonne National Laboratory, National Technical Director, ART FRP; and T.-L. Sham of Idaho National Laboratory, Technology Area Lead, Advanced Materials, ART Program.

The authors thank Zhili Feng and Lianshan Lin of ORNL for reviewing this report.

ABSTRACT

The Advanced Reactor Technologies (ART) Program has established a multi-year plan to develop Alloy 709 advanced stainless steel (A709), generate the data package and develop material-specific design parameters in qualifying it as a new structural material for Class A component design in the American Society of Mechanical Engineers (ASME) Boiler and Pressure Vessel Code, Section III, Division 5, High Temperature Reactors. In collaboration with material vendors, the Advanced Materials Development activities under ART have successfully scaled the A709 plate form production from a laboratory heat of 500 pounds to commercial heats totaling 133,000 pounds of A709 plate fabricated from three heats. The goal of the overall A709 development program is to establish the necessary microstructural and mechanical properties relationship for A709 to ultimately develop fabrication parameters for other product forms such as bars, piping and forging using the available ART A709 materials.

The objective of this A709 development work at ORNL in FY2023 is to experimentally determine grain coarsening behavior for the A709 heats and to experimentally generate the continuous cooling precipitation (CCP) diagram for A709 using the as-rolled commercial heat plate materials. Integral to this work is the characterization of the as-rolled materials and the determination of an effective solution annealing process. This report summarizes the work performed to identify the grain coarsening temperature for commercial heat 58776-3RB fabricated by G. O. Carlson and heat 529900-02 fabricated by Allegheny Technologies Incorporated (ATI) Flat Rolled Products.

1. INTRODUCTION

Nuclear energy is one of the leading energy options of producing continuous low-carbon electricity, thereby reducing greenhouse gas emissions over the course of the nuclear power plants' life-cycle. The Sodium Fast Reactor (SFR), with its ability to improve thermal efficiency, is becoming one of the leading advanced reactor concepts. Although SFR technology is relatively mature, there must be improvements in its capital cost and economic return before the private sector invests in large-scale, commercial deployment of SFRs. Advances in the mechanical performance of structural materials are critical to realize the improvement in the economics of fast reactors. One of the objectives of the Advanced Materials Development activities of the Advanced Reactor Technologies (ART) Program for the US Department of Energy (DOE), Office of Nuclear Energy (NE) is to provide the technical basis needed to support the regulatory requirements for structural materials for advanced reactors that could be deployed in the near-term to mid-term by the US nuclear industry.

Through a DOE-NE ART material down-selection and intermediate-term testing program, Alloy 709 (A709), an advanced austenitic stainless steel, was recommended as a Class A structural material for the SFR because of its overall superior structural strength advantage. A comprehensive Code qualification plan was developed to generate the data package and to develop material-specific design parameters required for Class A component design in ASEM Section III, Division 5 (Sham, *et al*., 2022). In collaboration with two US steel fabricators, DOE-NE ART successfully scaled up the production of A709 in plate form from a laboratory heat of 500 lb to commercial heat the first commercial heat of 45,000 lb in FY2017, fabricated by G.O. Carlson Inc of Pennsylvania. The second and third commercial heat were fabricated by Allegheny Technologies Incorporated, both in plate form, with a total weight of 41,000 lb and 38,000lb respectively. The ASME Code Cases testing efforts are being carried out on these three heats of A709 by at Oak Ridge National Laboratory (ORNL), Idaho National Laboratory (INL) and Argonne National Laboratory (Argonne).

The objective of the A709 development work is to establish thermomechanical processing – microstructure – mechanical properties relationships for A709 to develop fabrication parameters that can

be employed for product forms such as bars, pipes, and forgings in addition to plates. In FY2023, the focus of A709 development work at ORNL is to experimentally define the continuous cooling precipitation (CCP) diagram for A709 using the as-rolled commercial heat plate materials. However, prior to the CCP study, it is essential to determine the grain coarsening temperature for these specific heats. The grain coarsening temperature (T_{GC}) is the temperature at which there is significant enhanced grain growth due to the dissolution of pre-existing precipitates (carbides, carbonitrides, etc.) in the alloy that can pin grain boundaries. Research in this area has been important in the development of optimized thermomechanical processing of microalloyed steels in which precipitation during processing is highly controlled to develop a consistently uniform, fine-grained microstructure (Palmiere *et al*., 1996; Wang *et al.*, 2006; Solis-Bravo *et al*., 2020, Wang *et al*., 2021). The T_{GC} determination will be used for the subsequent CCP study to ensure maximum dissolution of pre-existing precipitates.

This report summarizes characterization of the as-rolled material and development of an effective solution annealing process, which is fundamental for the CCP study as well as for the development of effective thermomechanical processing parameters for Alloy 709. This study to experimentally determine the grain coarsening behavior and grain coarsening temperature was performed at the University of Pittsburgh using commercial heat 58776-3R fabricated by G. O. Carlson and heat 529900-02 fabricated by Allegheny Technologies Inc (ATI) Flat Rolled Products.

2. MATERIALS AND EXPERIMENTAL PROCEDURE

2.1 Materials And Processing

The as-rolled heat 58776-3R plate fabricated by G. O. Carlson (the Carlson Heat) had a nominal thickness of 1.1-inch, and as-rolled plate from heat 529900-02 fabricated by Allegheny Technologies Inc (the ATI Heat) had a nominal thickness of 1.75-inch. Table 1 shows the chemical compositions of the two heats with the final chemistry for the remelted product for the Carlson heat and product chemistry analysis for the ATI heat. For comparison, the specification for the chemical requirements of Nippon Steel NF709, TP310MoCbN seamless tubing, with a UNS number of S31025 in ASME SA-213 (ASME, 2021) is also listed in Table 1. Both commercial heats met the specified NF709 chemical requirements.

For both the as-rolled Carlson and ATI plates, approximately 1/4-in of as-received plate top and bottom surface layers were removed and discarded, and the remaining section was used for machining specimens for this study. The as-received Carlson heat samples had nominal dimensions of 6.3mm in the rolling direction, 16mm in the thickness direction and 19mm in the width direction of the original plate. The as-received ATI heat samples were 9mm in the rolling direction with the other two dimensions the same as the Carlson samples.

Table 2 lists the annealing temperatures and times used in this study. The selection of these heat treatments was based on the results of thermodynamic analysis for phase balance and precipitation dissolution temperatures using JMat Pro commercial software.

The grain coarsening experiments were conducted in a tube furnace capable of 1250°C annealing treatments. The samples were encapsulated in quartz under vacuum to avoid any oxidation during the anneals. After completing the annealing treatment, the samples were water-quenched (capsules broken) to minimize any precipitation during cooling.

Table 1. Chemical compositions of two commercial as-rolled A709 plates with heat number 58776-3R and 529900-02 (wt %)

Element	Carlson Heat (Heat 58776-3R)	ATI Heat (Heat 529900-02)	ASME SA-213 UNS-S31025 Specification
C	0.066	0.08	0.10 max
Cr	20.05	20	19.5–23.0
Co	0.02	0.02	–
Ni	25.14	24.6	23.0–26.0
Mn	0.9	0.9	1.50 max
Mo	1.51	1.5	1.0–2.0
N	0.152	0.16	0.10–0.25
Si	0.38	0.35	1.00 max
P	0.014	0.004	0.030 max
S	0.001	<0.001	0.030 max
Ti	**0.01**	**<0.01**	0.20 max
Nb	**0.26**	**0.17**	0.10–0.40
Al	0.02	0.01	–
B	0.003	0.005	0.002–0.010
Cu	0.06	0.07	–
Fe	Bal.	Bal.	Bal.

Table 2. Temperatures and times for the A709 heat treatments

Heat 58776 -3RB (Carlson heat)	----	1000°C 1h	1050°C 1h	1100°C 1h	1150°C 1h	1200°C 1h	1250°C 1h	1250°C 3h
Heat 529900 -02 (ATI heat)	950°C 1h	1000°C 1h	1050°C 1h	1100°C 1h	1150°C 1h	1200°C 1h	---	---

2.2 Specimen Preparation and Analysis Techniques

The as-received (as-rolled) and as-annealed and water-quenched samples were prepared for microstructural analysis using standard metallographic techniques. Samples were ground with abrasive paper (320, 400, 600, 800 and 1200 grid), polished with a 0.05µm alumina suspension and etched with a V2A solution to reveal the austenite grain boundaries and twins. V2A is a solution of 50 mL hydrochloric acid (HCl), 50 mL deionized water and 5 mL nitric acid (HNO_3). Samples were submerged from 5 to 20 minutes to reveal the grain boundaries, rinsed thoroughly, and dried prior to examination in a Zeiss Smart Zoom 5 light optical microscope (LOM).

Specimens were also examined in a Zeiss Sigma 500 VP (Variable Pressure) field emission gun (FEG) scanning electron microscope (SEM) equipped with an Oxford Instruments XMax80 Silicon Drift Detector (SDD) with an AZTEC analysis system and Oxford Instruments electron backscatter diffraction (EBSD) detector. All analyses were performed at 20 kV. The SEM examination of the etched specimens provided an indication of the effect of annealing temperature on precipitate dissolution.

EBSD data were acquired over an area 640 μm by 500 μm with a step size of 1.1 μm to assess both the coarser deformed grains as well as the intermediate recovered grains, and the very fine recrystallized grains present in the as-received plate. For several cases at high annealing temperatures, a larger area was acquired for EBSD data to collect statistical information on coarse grains. All EBSD data were processed using the Oxford Instruments EBSD software. The grain sizes obtained from the EBSD analyses were then plotted to show the grain size distribution for the as-received and as-annealed specimens and thus evaluate the grain coarsening behavior.

SEM-EDX spectrum imaging (SI) and discrete spot analyses were performed at 20 keV to qualitatively assess the presence of precipitates and inclusions in the as-received and as-annealed + water-quenched samples. Each spectrum image (SI) dataset was acquired for a live-time of ~10 minutes. These data provided a preliminary indication of the extent of precipitation as well as the presence of undissolved inclusions (ranging from approximately ~0.3 μm to several μm in size). SEM-EDX SI datasets were processed using the Oxford Instruments TruMap™ software.

3. RESULTS AND DISCUSSION

3.1 GRAIN COARSENING STUDY: CARLSON PLATE – HEAT 58776-3R

The as-received specimens from the Carlson Heat were in the as-rolled condition, thereby providing the baseline microstructure condition produced by Carlson. The grain coarsening test specimens were reheated according to the annealing matrix listed in Table 2. After the anneal, each specimen was water quenched.

3.1.1 As-Received Microstructure

LOM: The as-received material was highly inhomogeneous and contained partially recrystallized grains and coarse, elongated (deformed) grains surrounded by fine, recrystallized grains. The average grain size was approximately 25 μm in the as-received (as-rolled) condition; however, the grain size distribution was bi-model distribution. Thus, an "average" grain size for the as-received rolled plate does not provide a valid measure of the microstructure. The light optical micrographs revealed the presence of coarse elongated (>150 μm) grains as well as very fine (<10 μm) recrystallized grains. The light optical micrographs presented in Figure 1 provide examples of the non-uniform grain structure that characterized the as-received Carlson plate.

EBSD: The EBSD Inverse Pole Figure (IPF) map obtained from the as-received specimen (Figure 2) highlighted the highly inhomogeneous microstructure and provided data to generate the grain size distribution (frequency versus grain size, and area fraction versus grain size) presented in Figure 3. Many grains were less than 10 μm in diameter. This provides a more accurate description of the grain size compared to an "average grain size" due to the significant microstructural inhomogeneity in the as-received plate.

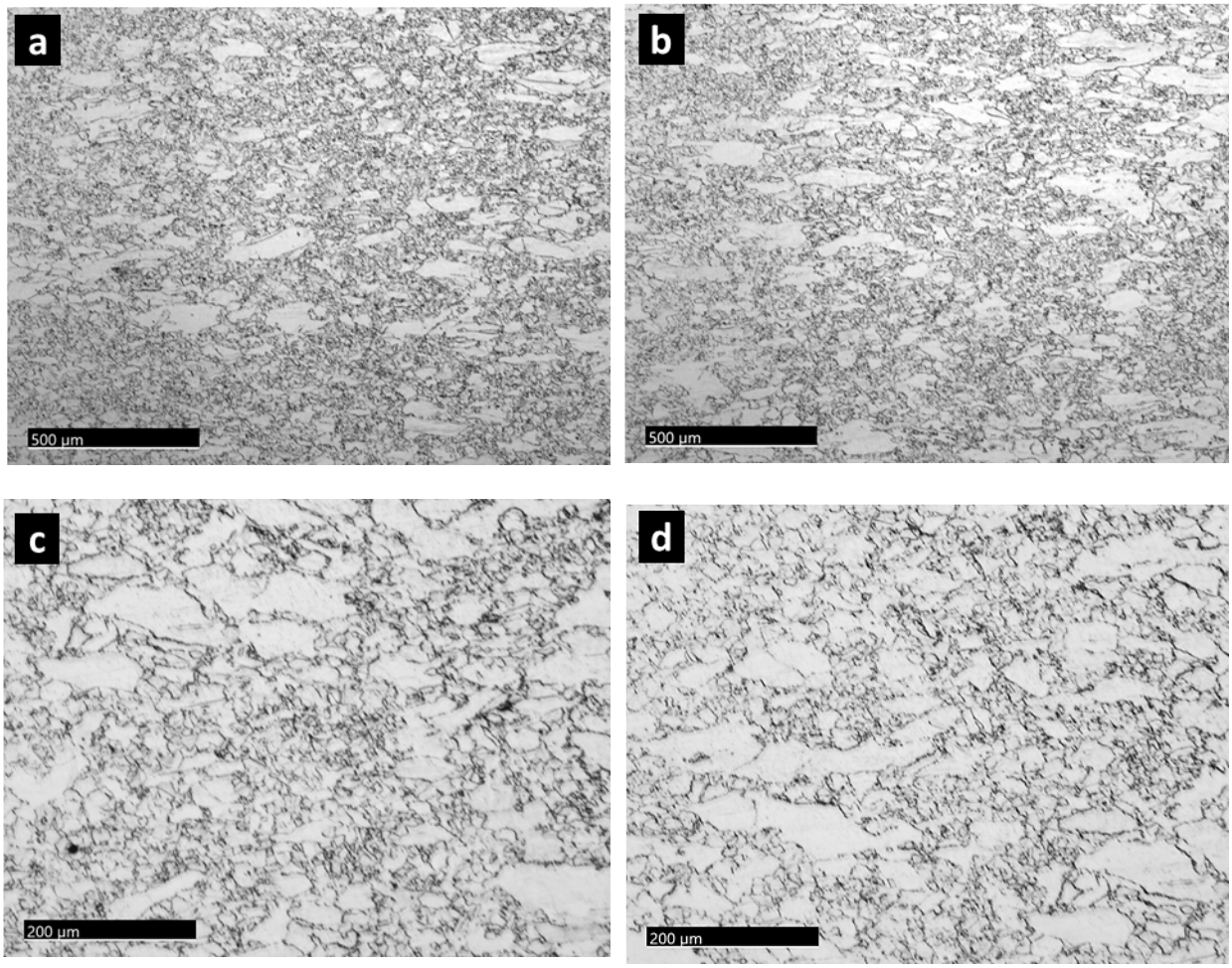

Figure 1. **(a)-(d) Representative optical micrographs of the as-received Carlson plate.**

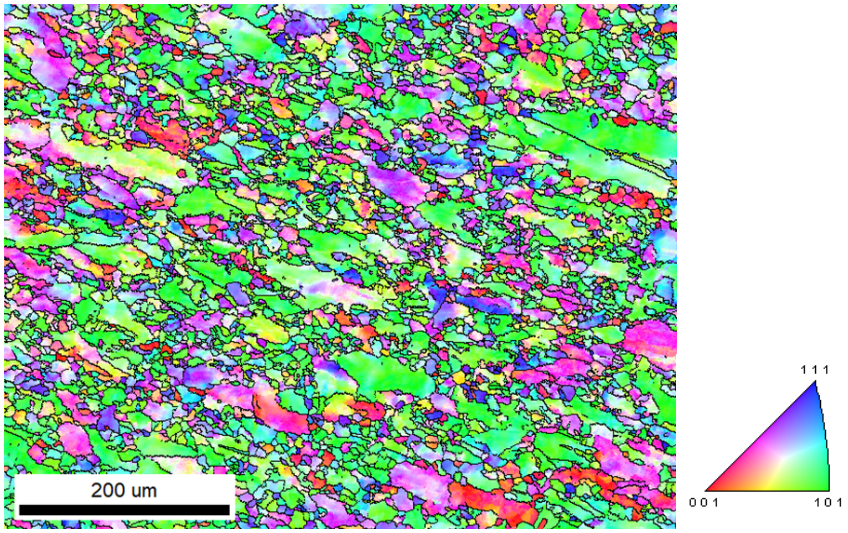

Figure 2. **EBSD IPF map of the as-received Carlson plate.**

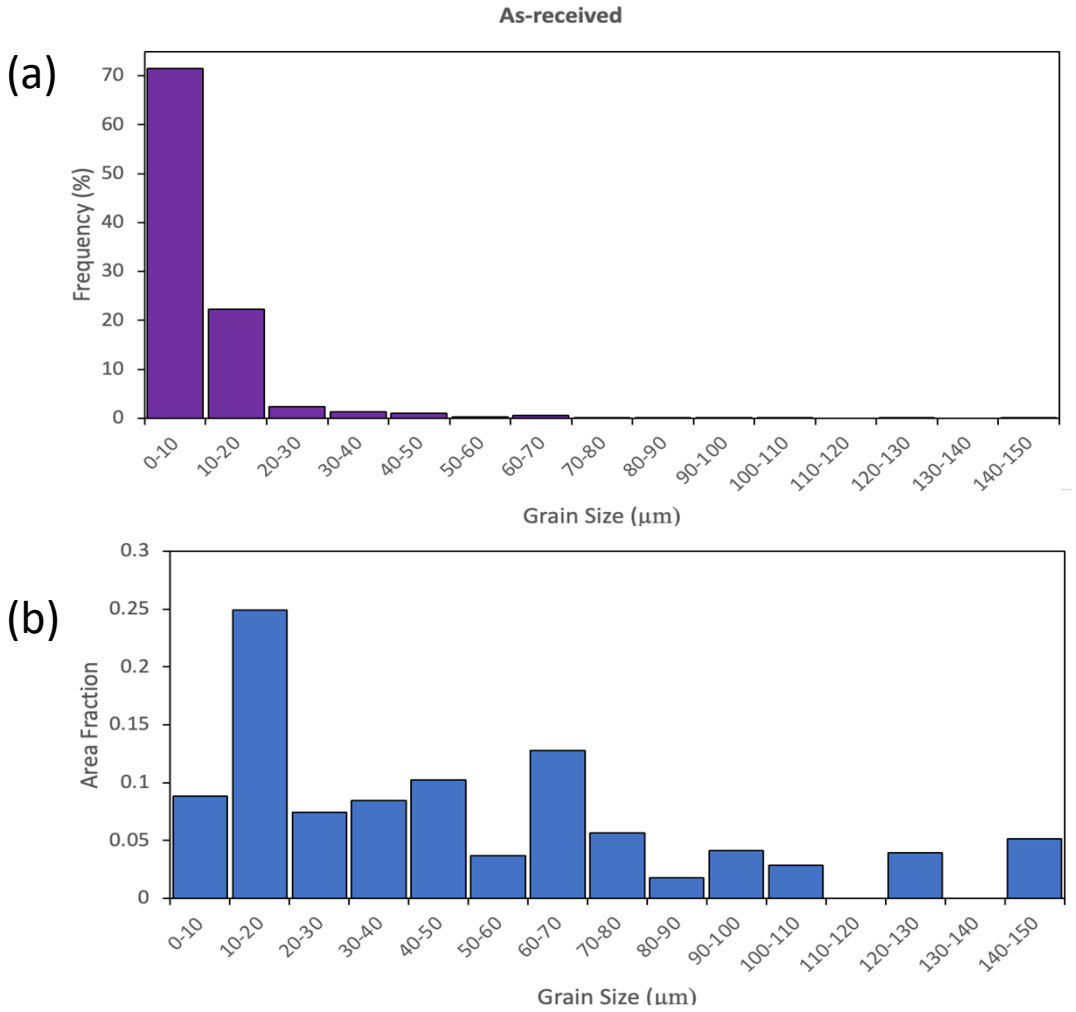

Figure 3. (a) Grain size frequency distribution and (b) grain size data plotted as a function of area fraction as measured from EBSD data obtained from the as-received Carlson plate.

3.1.2 Annealed and Water-Quenched Specimens

Microstructural characterization of these specimens provided information on the grain size evolution and qualitative analysis of precipitates present in the material.

1000°C/1h: This anneal promoted some recrystallization within the as-received rolled plate specimen as evidenced by the notable decrease in the proportion of elongated deformed grains that characterized the complex as-received plate microstructure. Representative optical micrographs are presented in Figure 4. The 1000°C heat treatment did induce some significant local changes in the microstructure associated with rapid recrystallization of some grains. A large local region resistant to the etchant was detected (see Figure 4 (b)) within this sample. Within this large region, smaller recrystallized regions were observed that appeared to be associated with small pre-existing inclusions. Furthermore, the shape of the boundary/interface between the "etched" and non-etched zone suggests that the recrystallization "front" was consuming the non-etched grains, which would indicate that the non-etched zone was deformed.

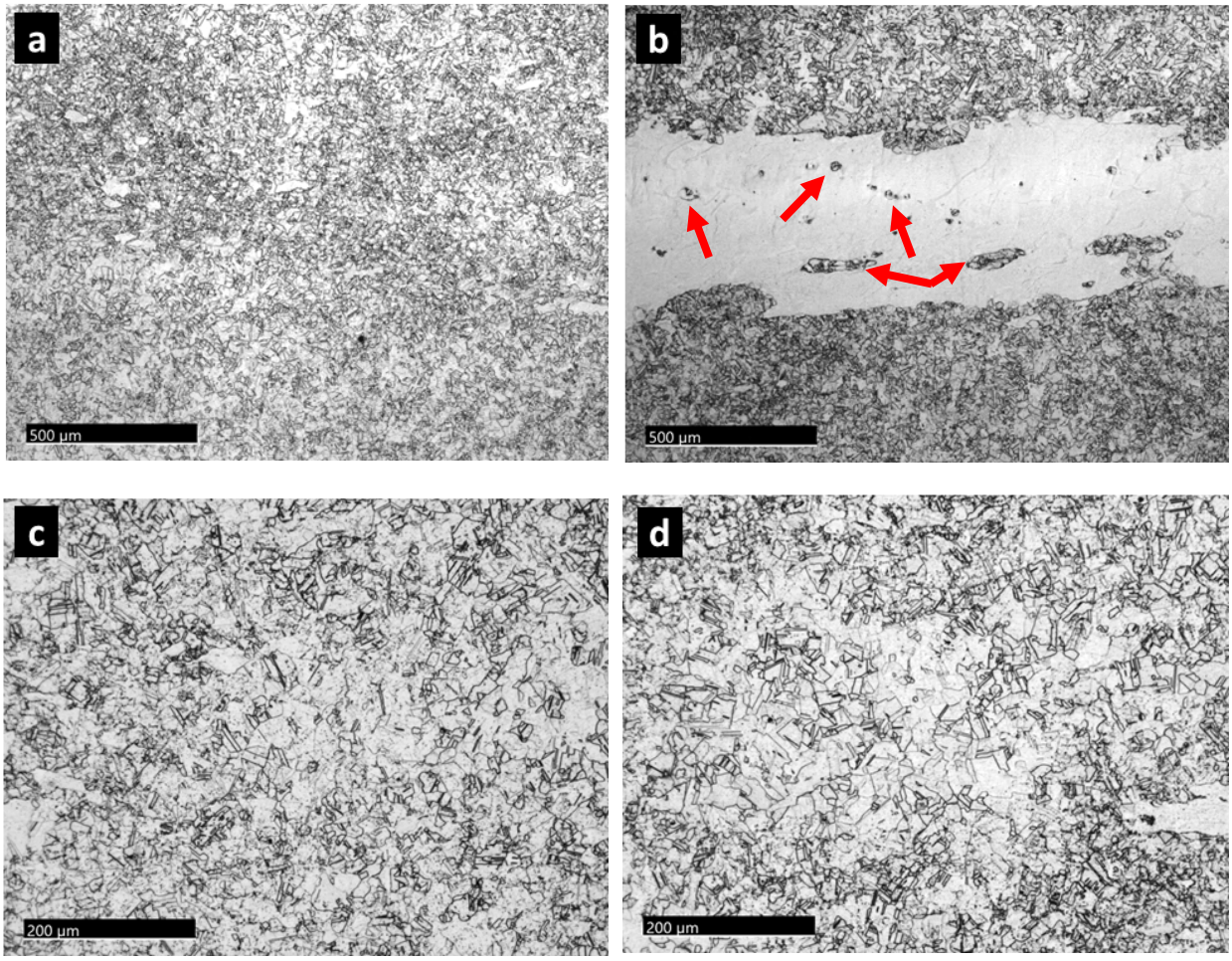

Figure 4. (a)-(d) Representative optical micrographs of the Carlson plate specimen annealed at 1000°C for 1 h and then water quenched. Note the high proportion of annealing twins with the fine recrystallized grains throughout the microstructure, and the presence of an abnormally large unetched zone shown in (b) that contains very fine, isolated recrystallized grains (red arrows).

The result of the EBSD analysis of the annealed and water-quenched plate sample is shown the inverse pole figure (IPF) in Figure 5. A large proportion of the recrystallized grains exhibited a [101] orientation. The EBSD data were also analyzed to generate the grain size distribution as well as the grain size versus area fraction plot. These are shown in Figure 6. The grain size distribution revealed an increase in the proportion of larger grains, and this is also reflected in the area fraction versus grain size plot.

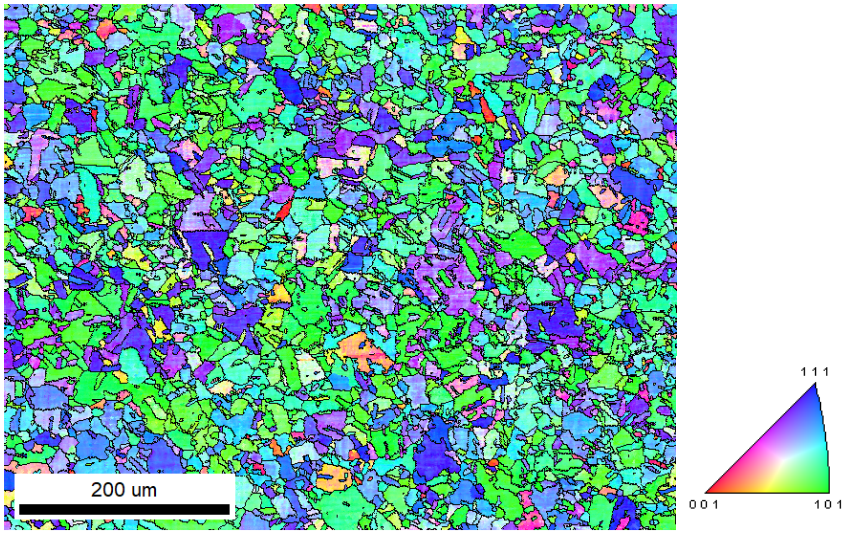

Figure 5. EBSD IPF map of the Carlson plate specimen annealed at 1000°C for 1 h.

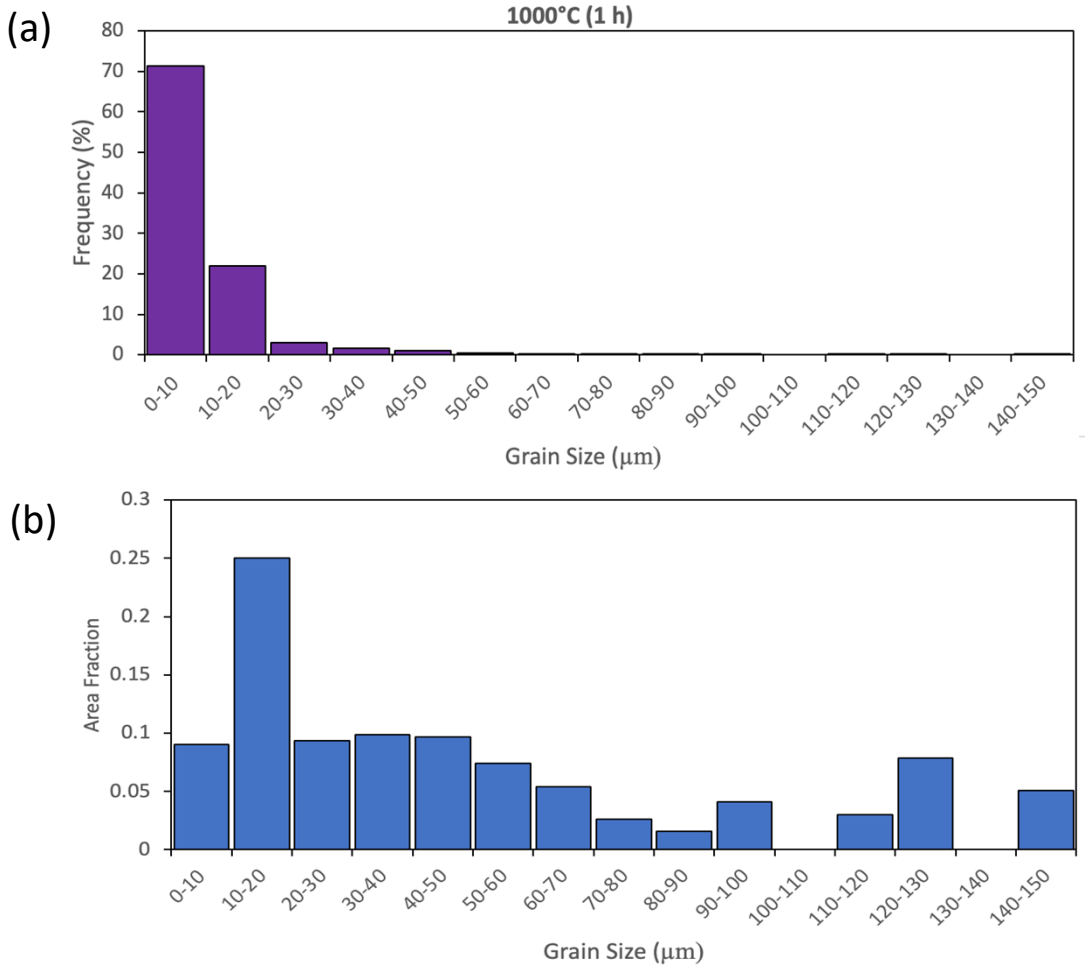

Figure 6. (a) Grain size frequency distribution and (b) grain size as a function of area fraction as measured from EBSD data acquired from the Carlson plate specimen annealed at 1000°C for 1 h.

1050°C/1h: This anneal promoted further recrystallization and some grain growth. Light optical metallographic evaluation still revealed a relatively fine microstructure, but areas with coarser recrystallized grains were also observed. Figure 7 contains representative micrographs of the etched annealed and water-quenched sample. A high proportion of twin boundaries were also observed within the recrystallized regions.

The EBSD data generated from this plate specimen is presented in the IPF in Figure 8. The EBSD data were used to obtain the grain size distribution and grain size versus area fraction plots included in Figure 9. Although there was still a high proportion of very fine grains, the area fraction of the 30-40 μm grains increased as the extent of recrystallization and grain growth continued.

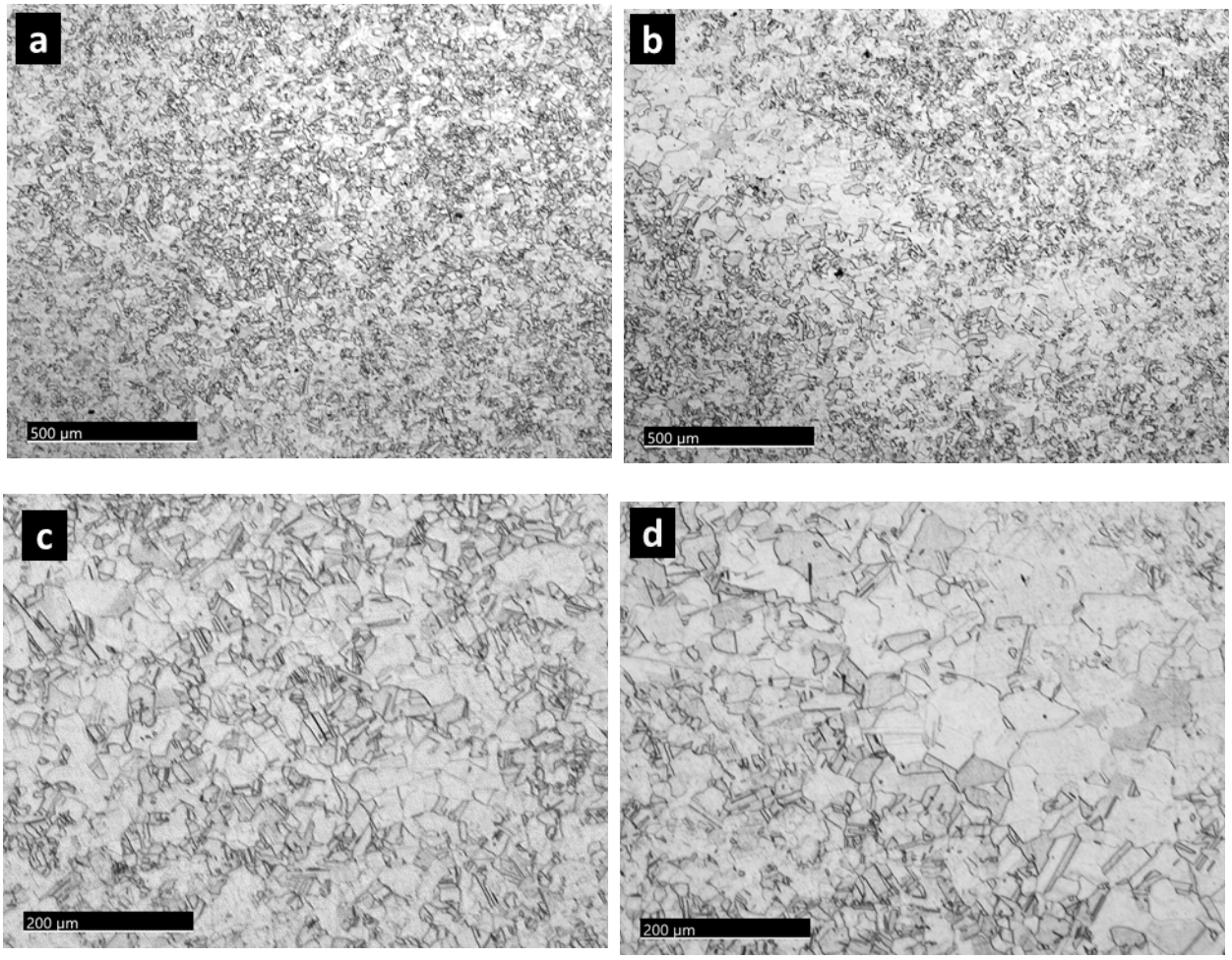

Figure 7. (a)-(d) Representative optical micrographs of the Carlson plate specimen annealed at 1050°C for 1 h. Note the variation in grain size evident in (c) and (d).

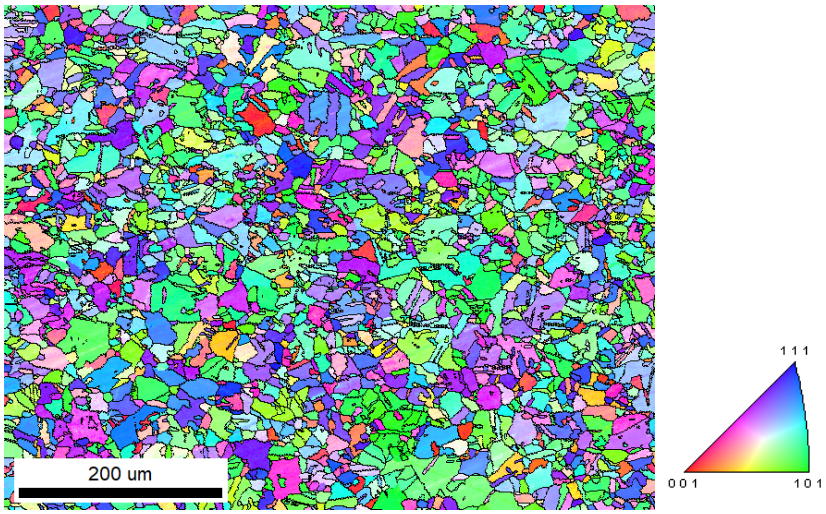

Figure 8. **EBSD IPF map of the Carlson plate specimen annealed at 1050°C for 1 h**

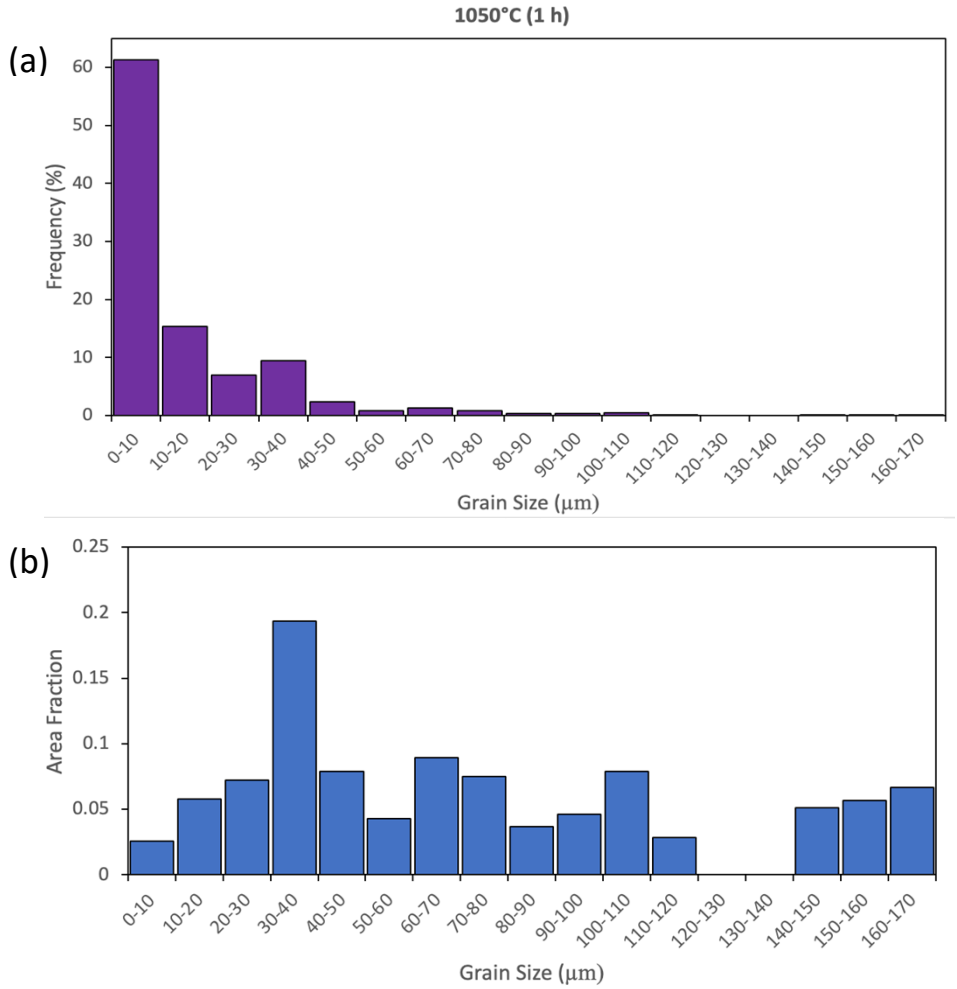

Figure 9. **(a) Grain size frequency distribution and (b) grain size as a function of area fraction as measured from EBSD data obtained from the Carlson plate specimen annealed at 1050°C for 1 h.**

1100°C/1h: This annealing treatment resulted in extensive recrystallization and grain growth. This can be observed in the optical micrographs in Figure 10, which show considerable variation in recrystallized grain size ranging from ~10-20 µm up to several hundred microns. Numerous annealing twins are evident throughout the microstructure. Some aligned inclusions consistent with the prior thermomechanical processing (rolling) were also observed (Figure 10 (d)).

The results of the EBSD analysis are presented in the IPF in Figure 11. Analysis of EBSD data for the grain size determination are included in the grain size distribution and area fraction plots shown in Figure 12. Although over 90% of the grains analyzed were ~50 µm or less, several large grains skewed the grain size versus area fraction plot, highlighting the issue of significant inhomogeneity in grain size within this annealed plate specimen.

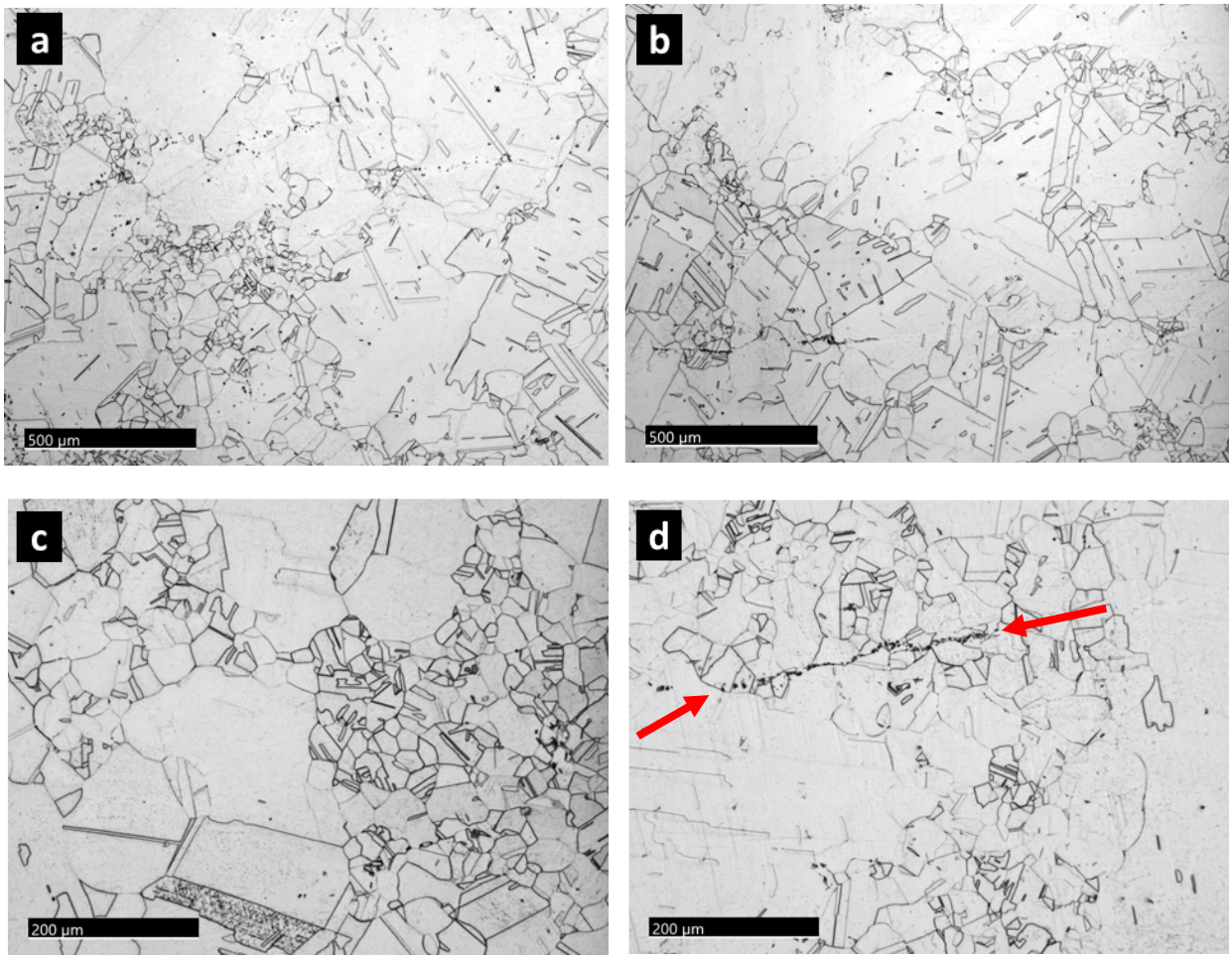

Figure 10. **(a)-(d) Representative optical micrographs of the Carlson plate specimen annealed at 1100°C for 1 h. Note the significant variation in grain size within the annealed plate. Some stringered inclusions are highlighted (red arrows) in (d).**

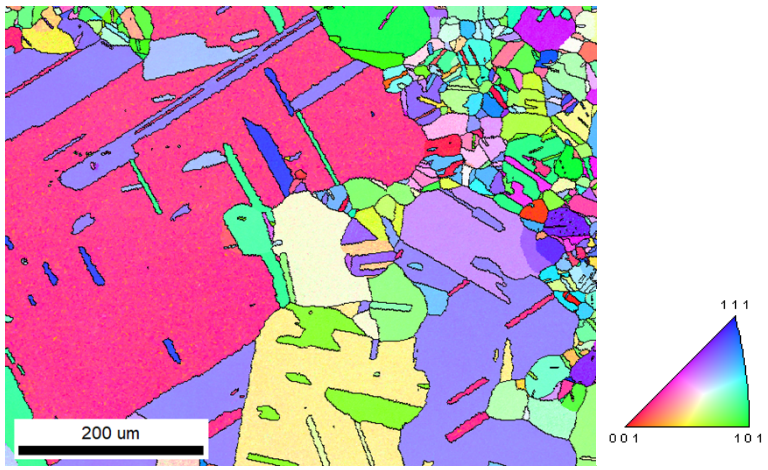

Figure 11. EBSD IPF map of the Carlson plate specimen annealed at 1100°C for 1 h.

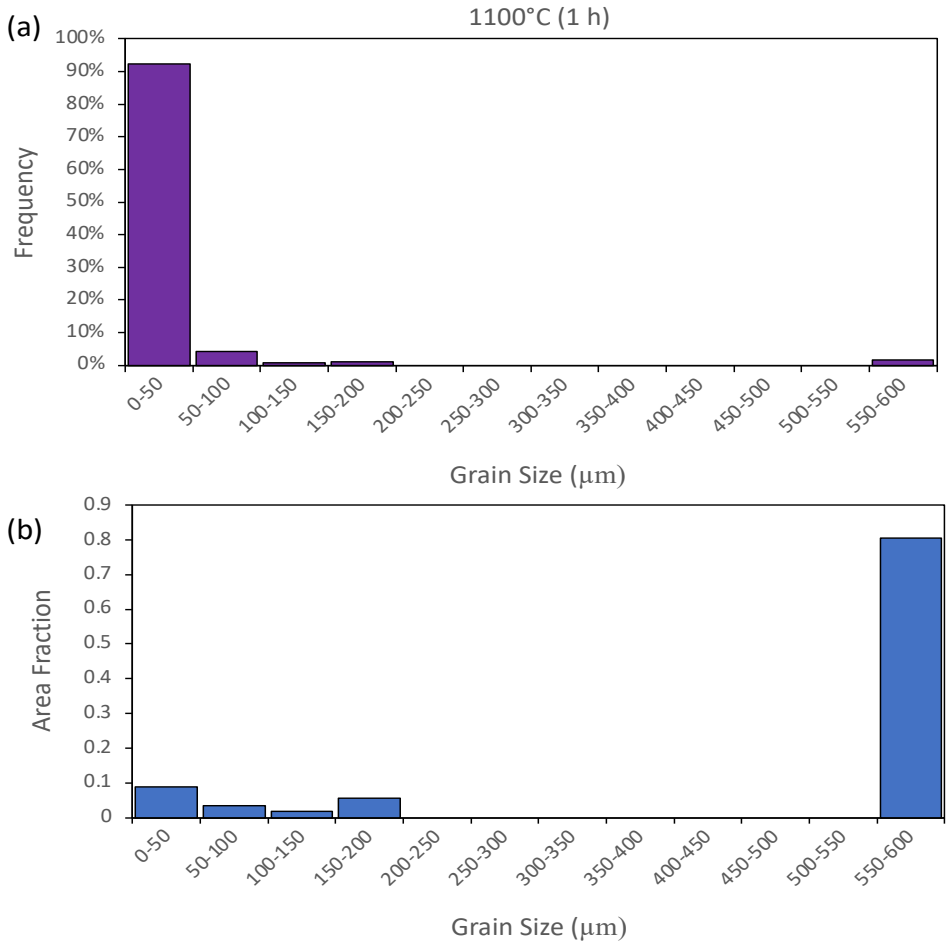

Figure 12. (a) Grain size frequency distribution and (b) grain size as a function of area fraction as measured from EBSD data obtained from the Carlson plate specimen annealed at 1100°C for 1 h. Note that the presence of very few coarse (>500 μm) grains significantly skews the area fraction.

1150°C/1h: The 1150°C annealing treatment resulted in a fully recrystallized microstructure as evidenced via optical metallographic examination. The representative optical micrographs shown in Figure 13 (a) and (b) provide examples of the nonuniformity in grain size within the annealed plate sample. The microstructure was also characterized by the presence of numerous annealing twins. Discrete inclusions were also observed throughout the material.

The EBSD IPF map generated from the EBSD data is presented in Figure 14. Figure 15 includes the grain size distribution and the grain size versus area fraction data plots that were based on EBSD characterization. The 1150°C anneal resulted in an increase in grain sizes, with a high proportion of the grain in the 50 to 100 μm size range, although some ~200 to 300 μm grains were also detected.

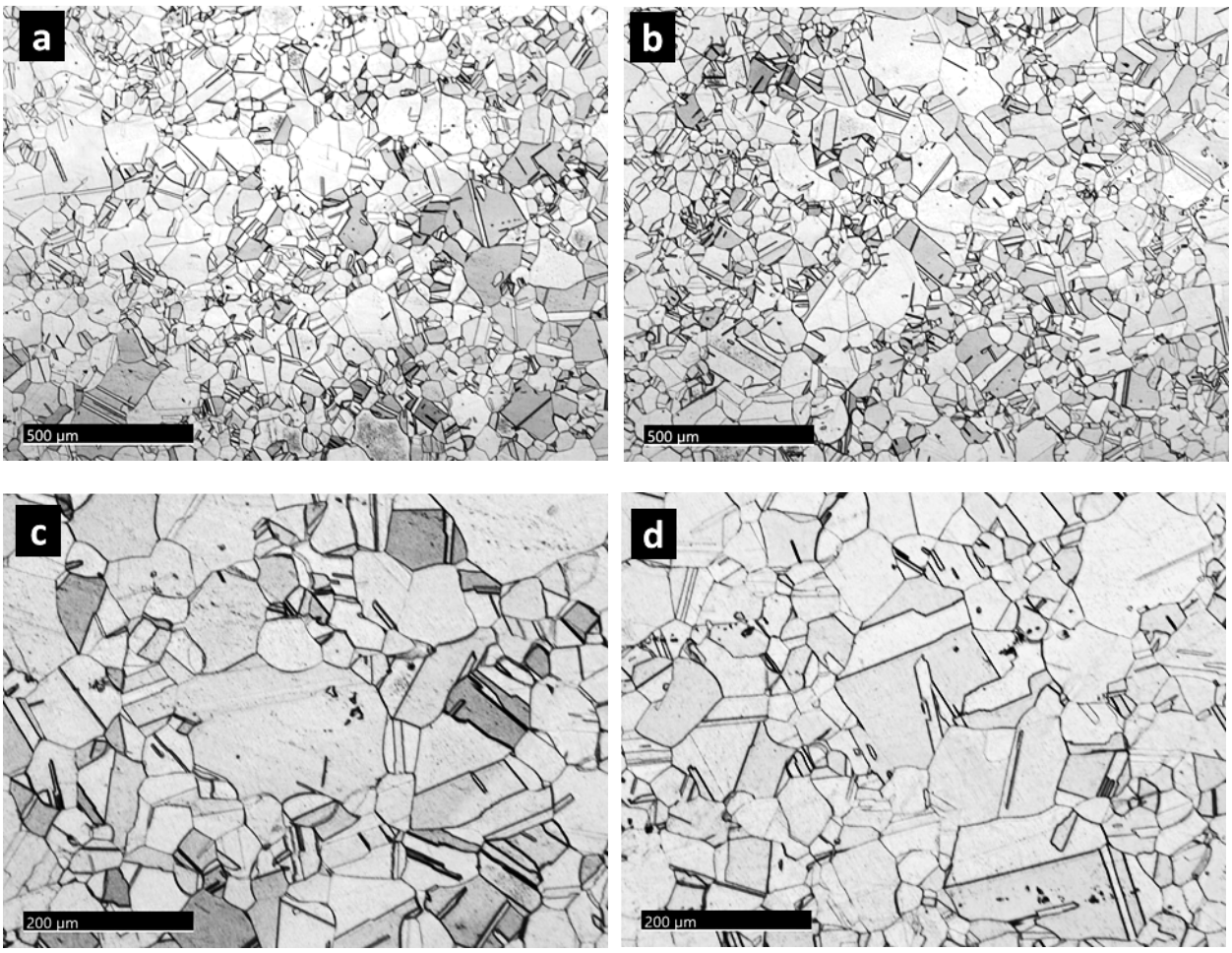

Figure 13. (a)-(d) Representative optical micrographs of the Carlson plate specimen annealed at 1150°C for 1 h. Note that the remnants of a "necklace structure" can still be observed in the lower magnification micrographs (a) and (b).

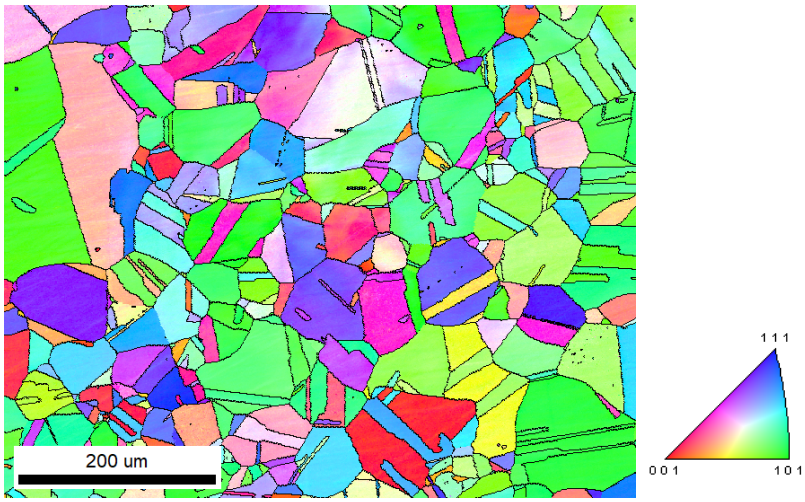

Figure 14. EBSD IPF map of the Carlson plate specimen annealed at 1150°C for 1 h.

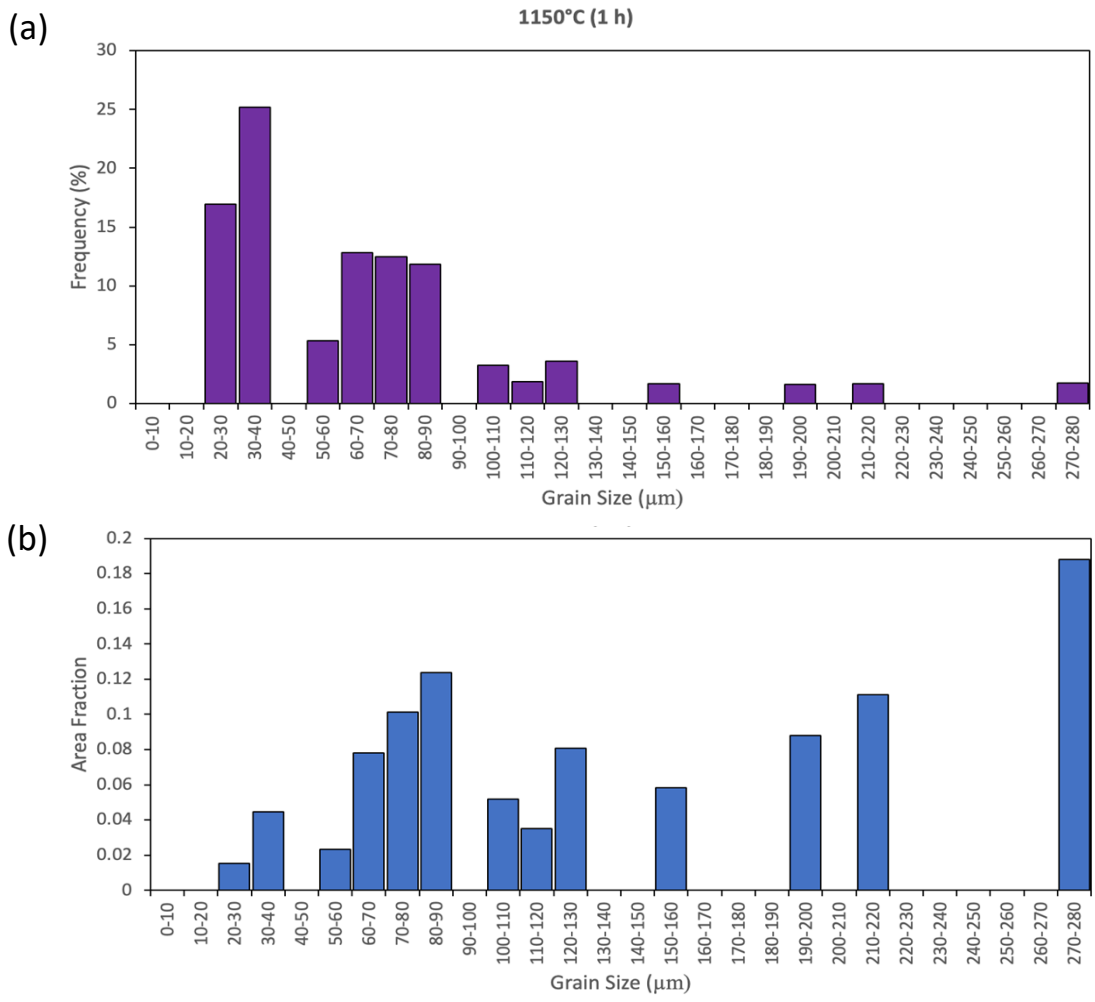

Figure 15. (a) Grain size frequency distribution and (b) grain size as a function of area fraction as measured from EBSD data obtained from the Carlson plate specimen annealed at 1150°C for 1 h.

1200°C/1h: The 1200°C anneal resulted in a fully recrystallized microstructure characterized by numerous anneal twins and a notable variation in grain size as shown in the optical micrographs of Figure 16. The inhomogeneous as-received microstructure of the plate is reflected in the microstructure even after a high temperature solution anneal. Also evident within the microstructure are discrete micron/submicron-size inclusions (see Figure 16 (c) and (d)).

The EBSD data are presented in the IPF of Figure 17. Again, the numerous annealing twins and recrystallized grain structure can clearly be observed. The grain size distribution and grain size versus area fraction data were extracted from the EBSD data and are presented in Figure 18. Note the broad grain size distribution, ranging from ~30 μm to over 500 μm. Figure 18 (a) shows a bimodal distribution in grain size, further confirming the inhomogeneous microstructure. The area fraction vs. grain size reflects the presence of a few very coarse grains in the dataset, demonstrating the nonuniformity in the as-annealed plate specimen.

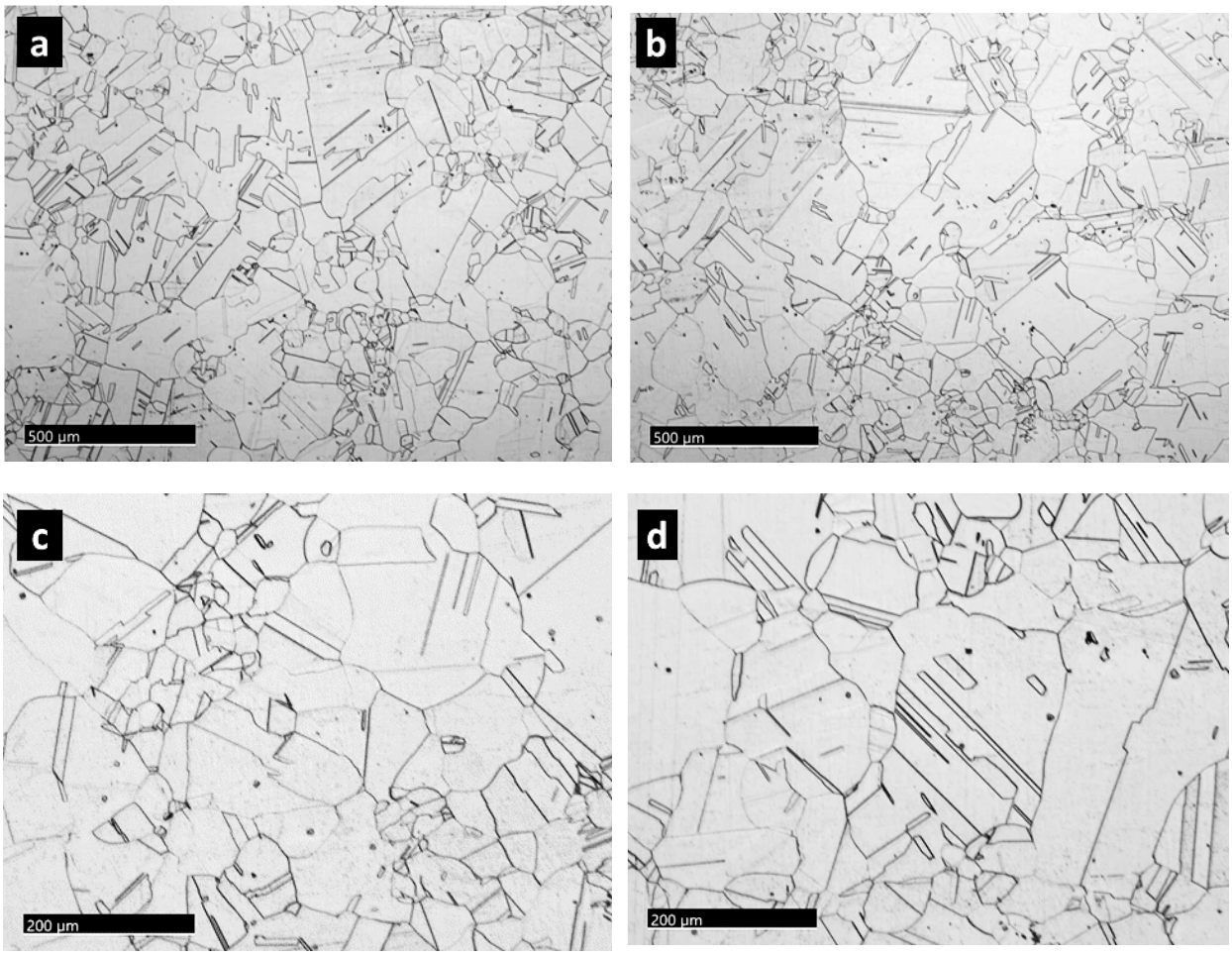

Figure 16. (a)-(d) Representative optical micrographs of the Carlson plate specimen annealed at 1200°C for 1 h.

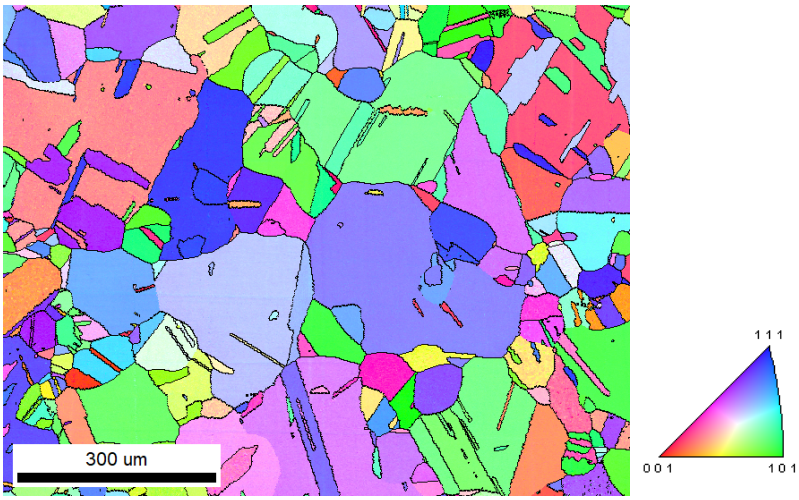

Figure 17. EBSD IPF map of the Carlson plate specimen annealed at 1200°C for 1 h.

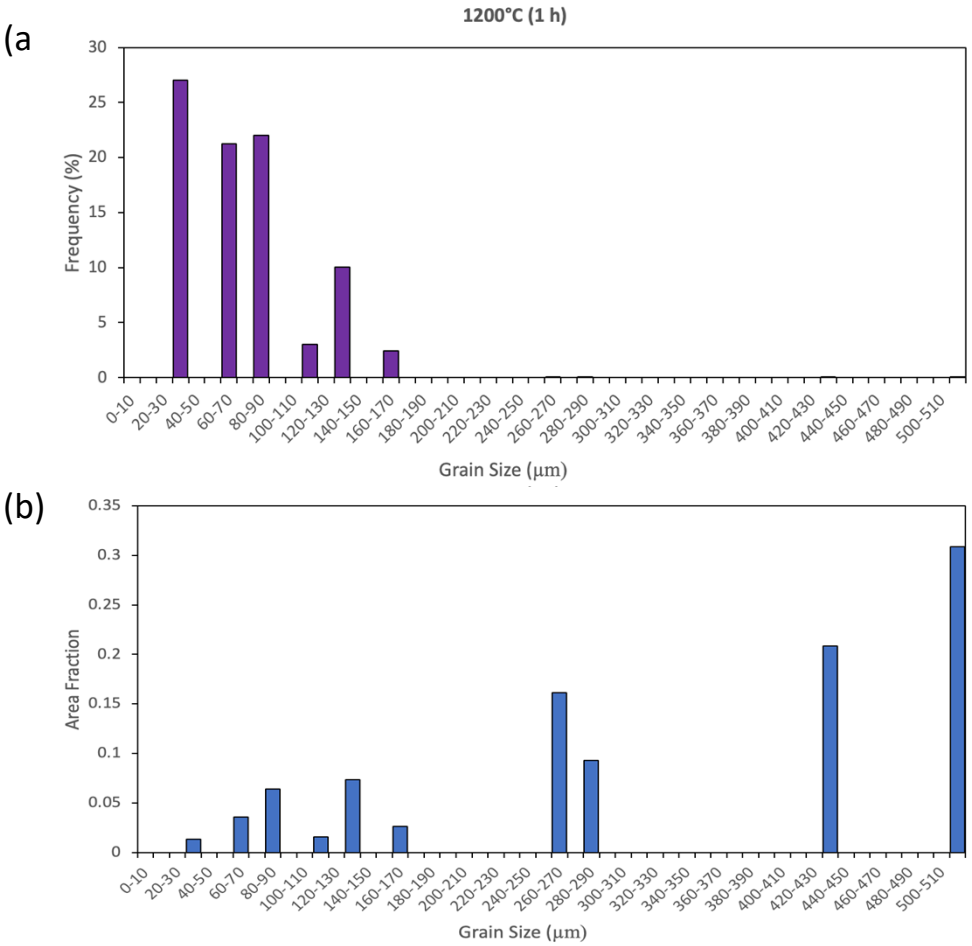

Figure 18. (a) Grain size frequency distribution and (b) grain size as a function of area fraction as measured from EBSD data obtained from the Carlson plate specimen annealed at 1200°C for 1 h.

1250°C/1h: A fully recrystallized equiaxed grain structure was produced during the 1 h anneal at 1250°C as shown in the optical micrographs presented in Figure 19. In addition to the numerous twins, discrete inclusions are also evident in these images.

The IPF generated from the EBSD data is shown in Figure 20. Figure 21 contains the results of the grain size distribution and grain size versus area fraction data extracted from the EBSD data. Examination of Figure 21 (a) reveals a bimodal grain size distribution after the 1250°C anneal.

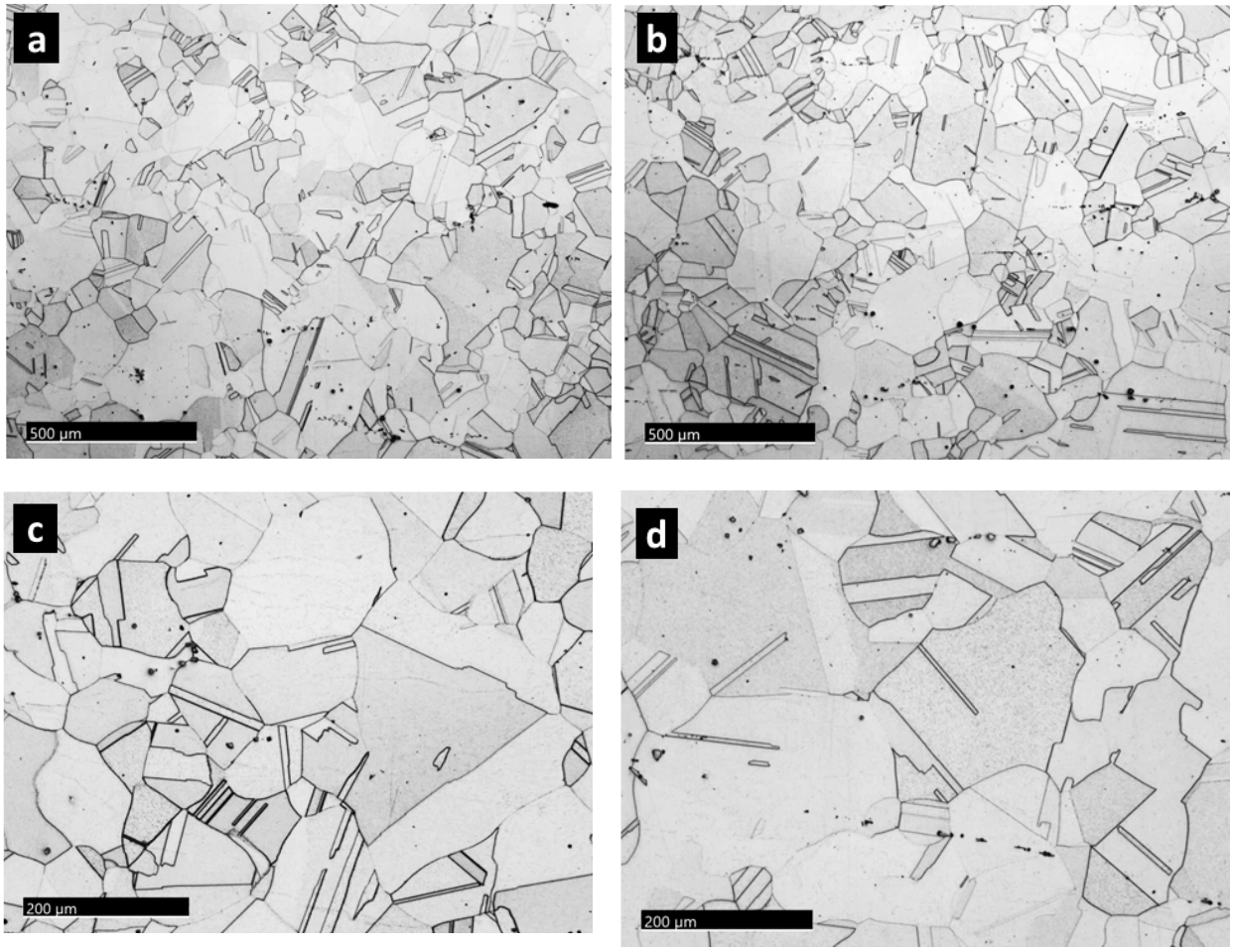

Figure 19. (a)-(d) Representative optical micrographs of the Carlson plate specimen annealed at 1250°C for 1 h.

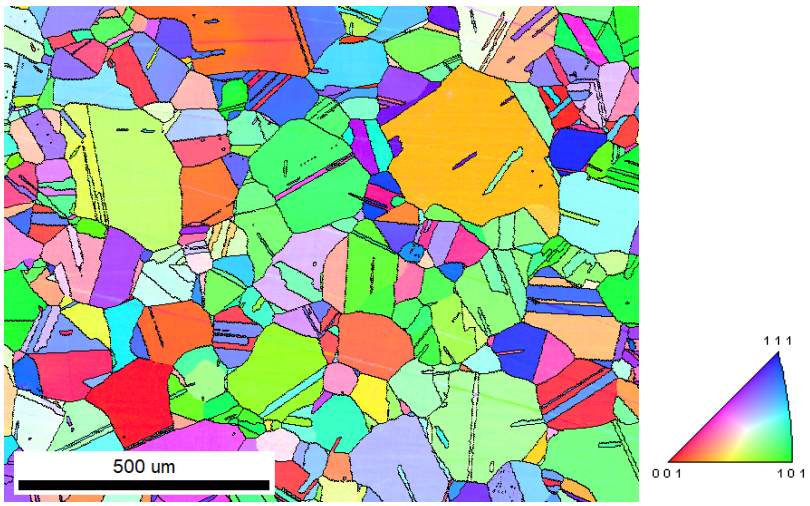

Figure 20. EBSD IPF map of the Carlson plate specimen annealed at 1250°C for 1 h

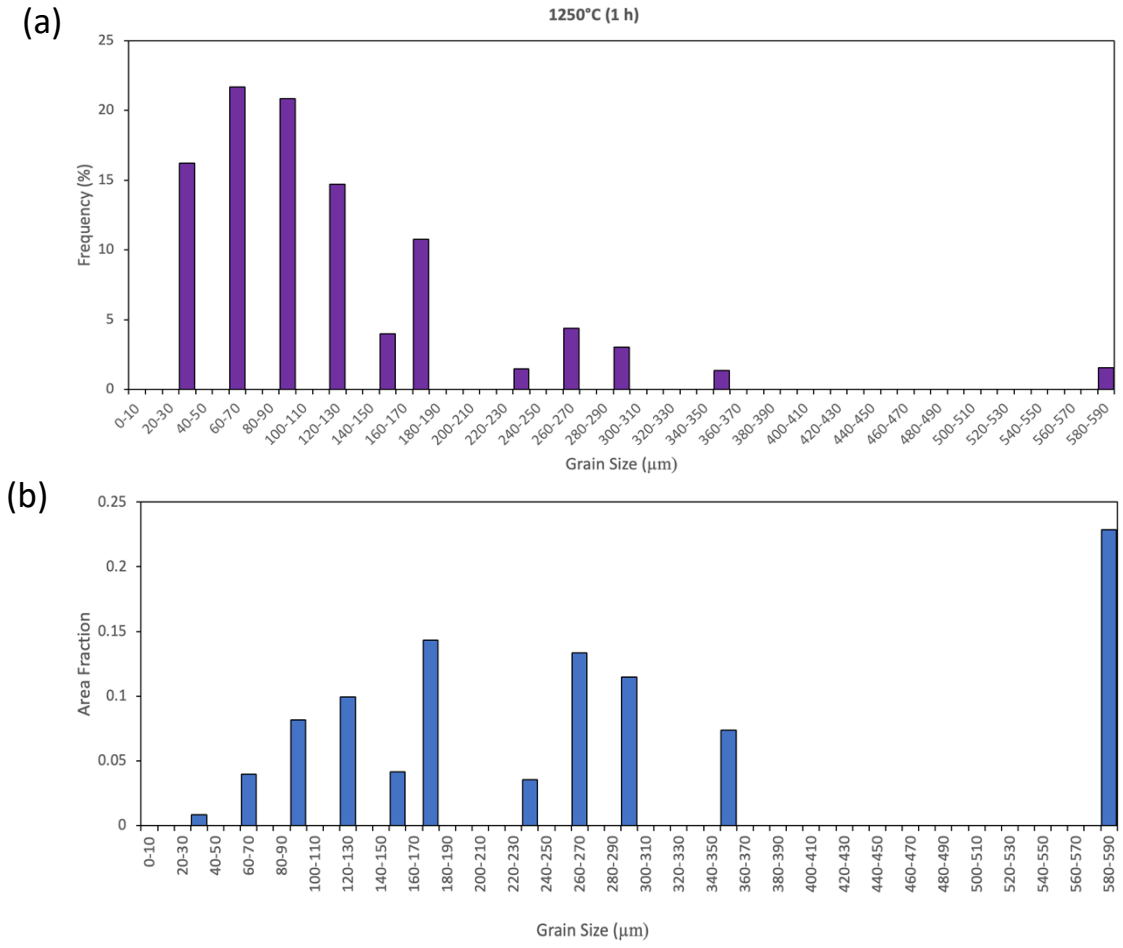

Figure 21. (a) Grain size frequency distribution and (b) grain size as a function of area fraction as measured from EBSD data obtained from the Carlson plate specimen annealed at 1250°C for 1 h.

1250°C/3h: Extending the anneal at 1250°C for 3 h did not have a significant effect on the microstructure. Both fine (~40-50 μm) and coarse (200+ μm) recrystallized equiaxed grains were observed, as shown in the optical micrographs of Figure 22. Discrete undissolved inclusions were also detected throughout the microstructure, some of which appeared to be clustered (Figure 22 (a) and (b)) or aligned (Figure 22(d)). These inclusions, formed during solidification, cannot be removed by long-term, high temperature anneals.

The EBSD data are presented in the IPF of Figure 23. Numerous annealing twins are evident throughout the IPF map. Also, the variation in grain size is evident in the IPF map. This variation in grain size is also shown in the grain size distribution data and grain size versus area fraction data of Figure 24. Note that these data reveal a finer minimum grain size compared to the data for the 1 h anneal at 1250°C, which further highlights the grain size inhomogeneity within the plate.

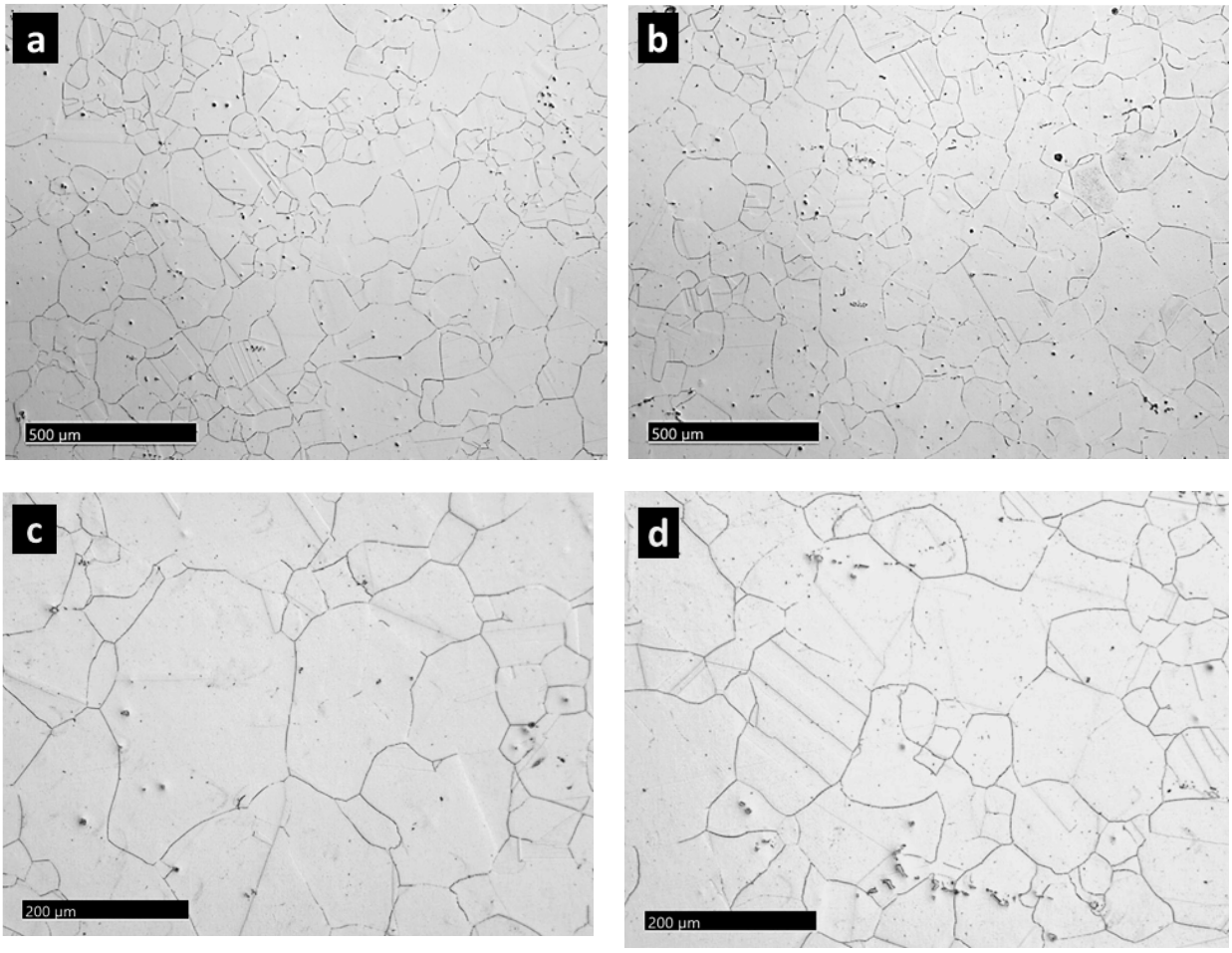

Figure 22. **(a)-(d) Representative optical micrographs of the Carlson plate specimen annealed at 1250°C for 3 h.**

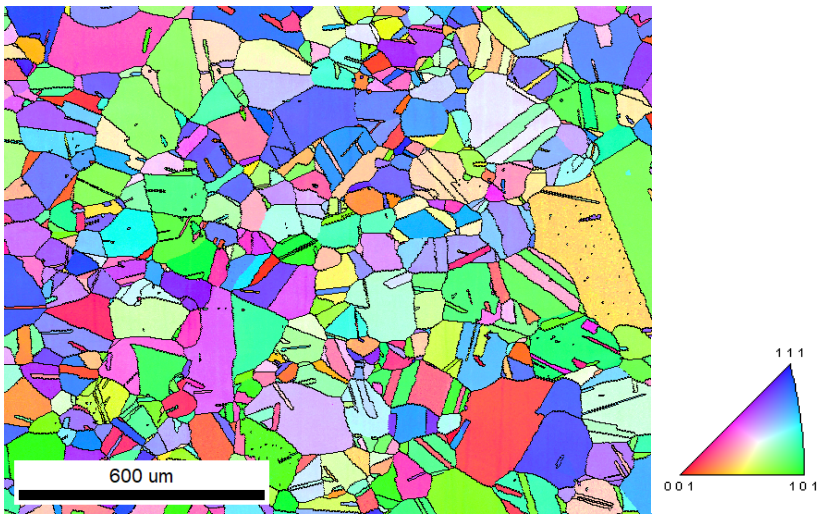

Figure 23. EBSD IPF map of the Carlson Heat specimen annealed at 1250°C for 3 h.

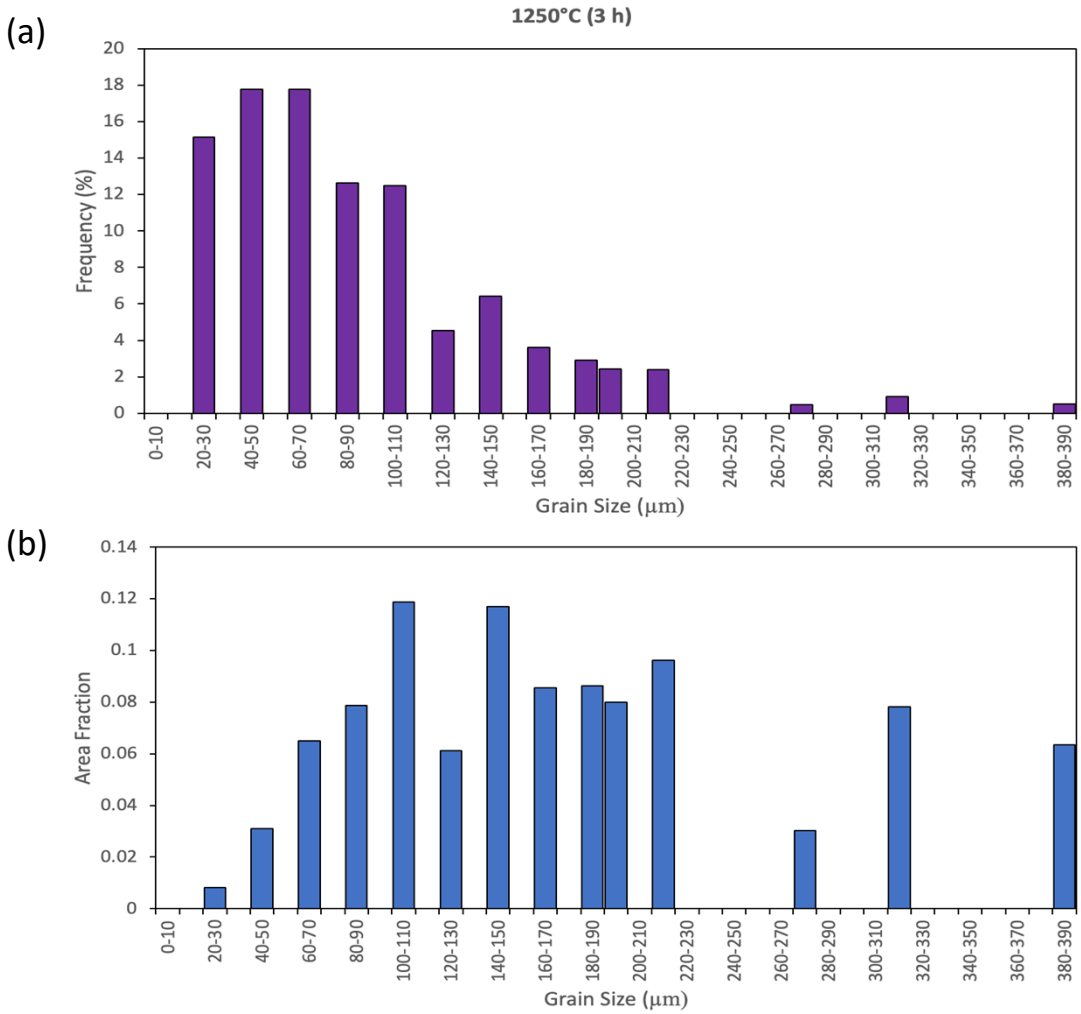

Figure 24. (a) Grain size frequency distribution and (b) grain size as a function of area fraction as measured from EBSD data obtained from the Carlson Heat specimen annealed at 1250°C for 3 h.

General: A summary of the grain size evolution as a function of the reheating/annealing conditions determined by EBSD analyses is shown in Figure 25. The average grain size measured for each specimen, including the as-received, as-rolled Carlson plate, is presented in Figure 25 (a). The standard deviation for each specimen is illustrated as the error bar on the average grain size for each annealing treatment. Note the extensive spread in the standard deviations, indicating the significant variation in grain size. This further demonstrates the importance of the grain size distribution to assess material homogeneity in microstructure as opposed to an average grain size for A709. It also reflects the fact that the significant inhomogeneity in the as-rolled plate cannot be fully eliminated by high temperature annealing.

Grain growth was evident at 1150 ºC and above. Interestingly, a comparison of the specimens annealed at 1250 ºC for 1h and 3h revealed that no significant difference in average grain size due to the increased annealing time. The significant variation in grain size in the annealed specimens is also reflected in the accumulated area fraction versus annealing temperature plot of Figure 25 (b). However, as shown by the grain size versus area fraction data, the presence of a few very coarse grains has a significant effect on the shape of the accumulated area fraction versus annealing/reheating temperature.

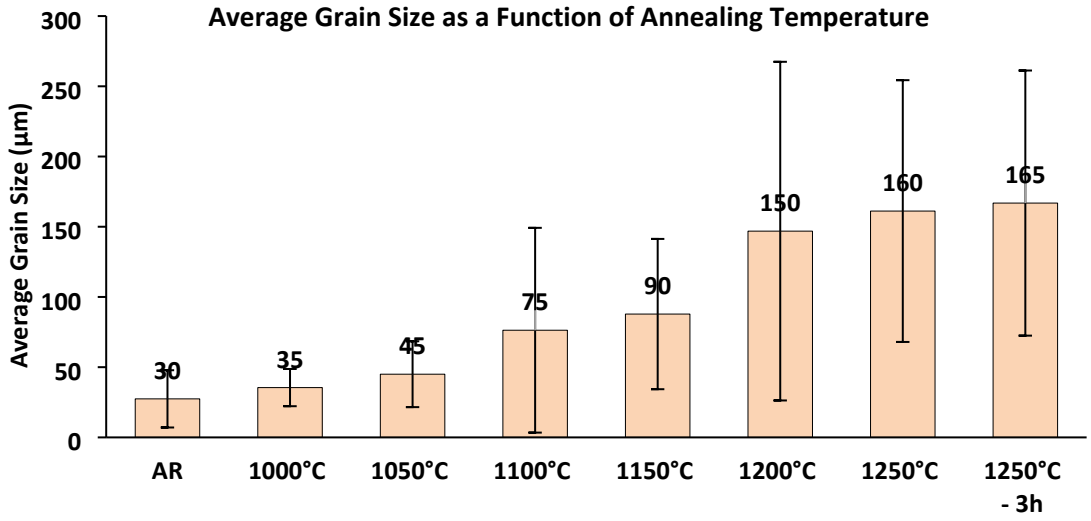

(a)

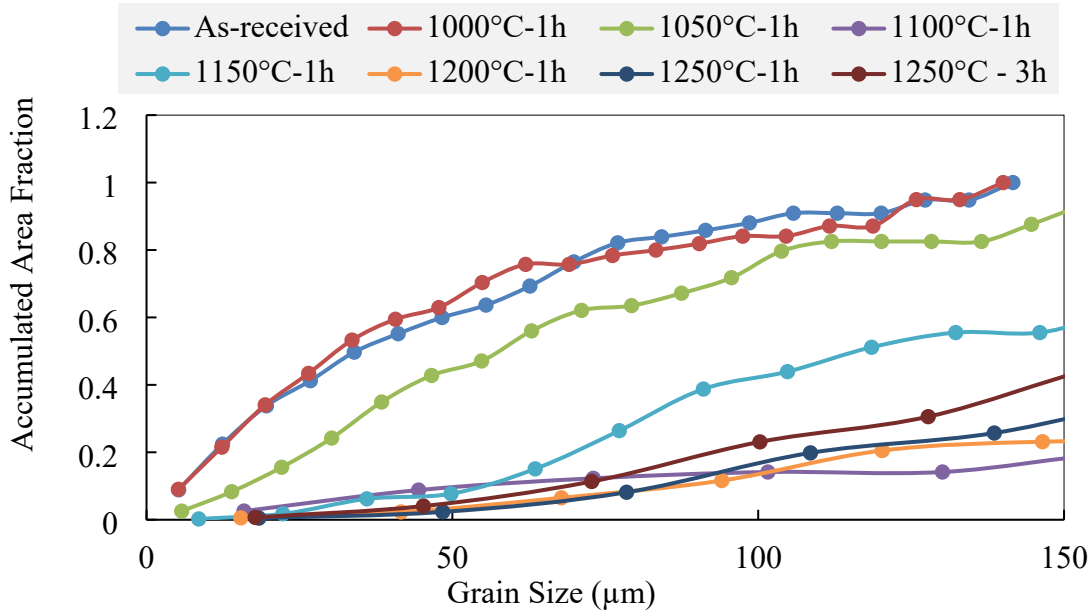

(b)

Figure 25. Summary of grain coarsening behavior for the Carlson plate from heat 58776 -3R with the results from EBSD analysis for various annealing conditions. (a) Average grain size (with standard deviation) as a function of annealing treatment; (b) Accumulated area fraction of grains as a function of grain size. The unusual behavior of the 1100°C specimen reflects the presence of a few extremely coarse (>500 µm) grains that impact the plot, as shown in Figure 12.

3.1.2 Preliminary FEGSEM-EDXS Analyses of As-Received and As-Annealed Carlson Heat 58776-3R Plate Specimens

Scanning Electron Microscopy (SEM) and Energy-dispersive X-ray spectroscopy (EDXS) were used to qualitatively assess the presence and dissolution of precipitates after each reheating/annealing treatment. It should be noted that this study is not intended to achieve quantitative measurements of the size, type, and volume fraction of precipitates, but to *qualitatively* provide an indication of relative precipitate dissolution behavior after reheating to the various annealing temperatures.

Figure 26 contains representative SEM-EDXS maps and EDX spectra extracted from the SEM-EDX spectrum imaging (SI) dataset obtained from the as-received Carlson plate sample. Coarse inclusions/ precipitates were randomly distributed along the austenite grain boundaries and throughout the matrix. The coarse inclusions appeared to be predominantly TiN, which served as preferential nucleation sites for (Nb,Mo)C carbides, and other complex CrNbMo-enriched carbides. It is noted that TiN will nucleate on the first inclusions to form in the melt, which tend to be Al_2O_3 or MgO – or a mixture of both. Thus, the presence of Al-rich oxide core is commonly observed within TiN inclusions in steels and Ni-base alloys.

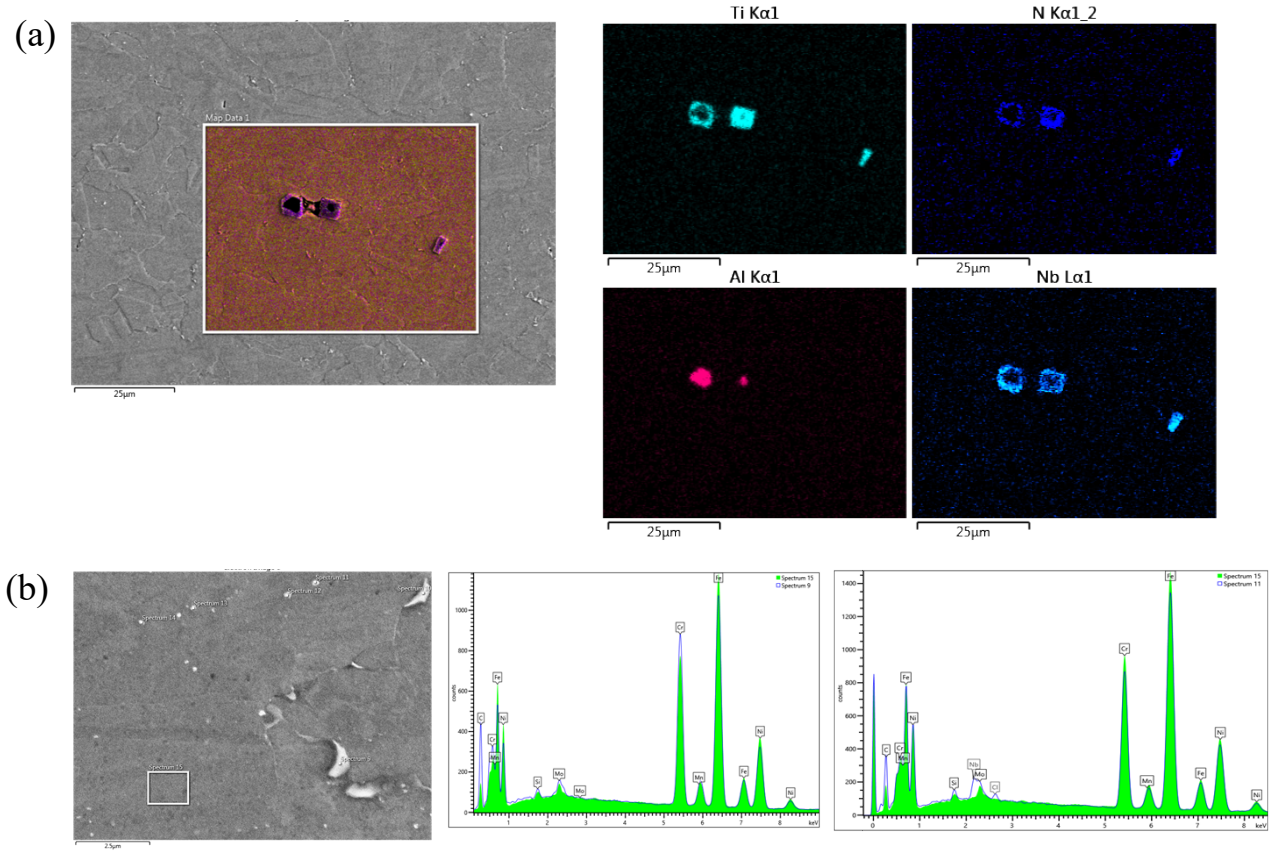

Figure 26. (a) SE image with superimposed elemental EDX map and individual EDX maps obtained from the as-received Carlson heat 58776 -3R. Note the presence of Ti, N and Nb surrounding the Al-enriched oxide core. (b) SE image of brightly-imaging precipitates and white box delineating the 'matrix' region for comparison with the EDX spectra obtained from the precipitates. The 'matrix' spectrum is green. (b) EDX spectrum of a coarse Cr-Mo-enriched carbide (blue line spectrum) and (c) EDX spectrum from a Nb-enriched carbide (blue line spectrum).

A comparison of the as-received and 1250°C/1 h microstructures for the Carlson plate samples is shown in Figure 27. Submicron Nb-Ti-enriched inclusions (possibly (Nb,Ti)(CN)) were also observed throughout the austenite. Figure 27 provides an example of fine submicron inclusions observed in the microstructure of the as-received sample after the 1250°C-1h anneal. At 1250°C, the (Cr, Mo)-enriched carbides appear to have dissolved, but the complex TiNb-enriched inclusions remained in the austenite matrix even after 3h at 1250°C (Figure 28).

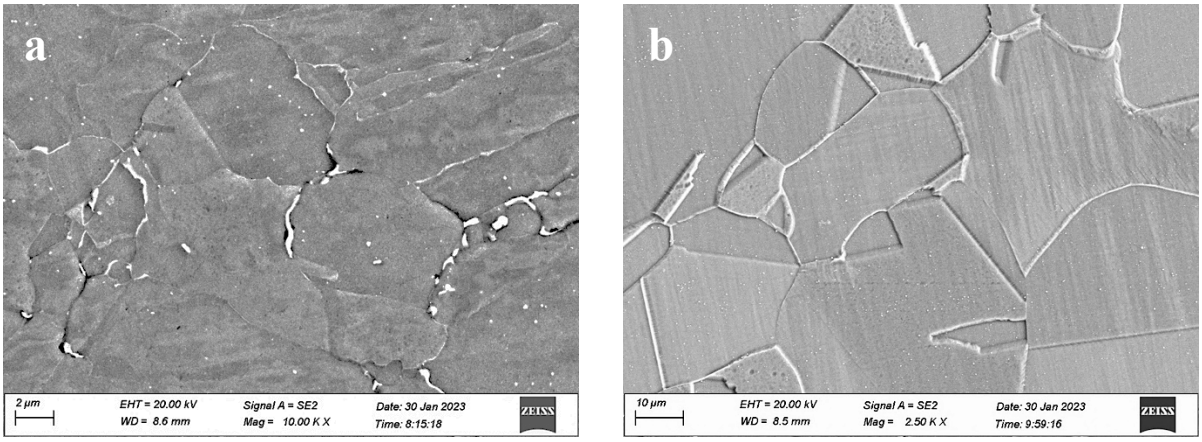

Figure 27. **SE images of the etched Carlson plate: (a) as-received condition; and (b) after 1 h at 1250°C and a water-quench. Note the absence of intergranular precipitates and a significantly coarser recrystallized grain structure after the 1250°C anneal. Some very fine, submicron inclusions may be observed within the grains.**

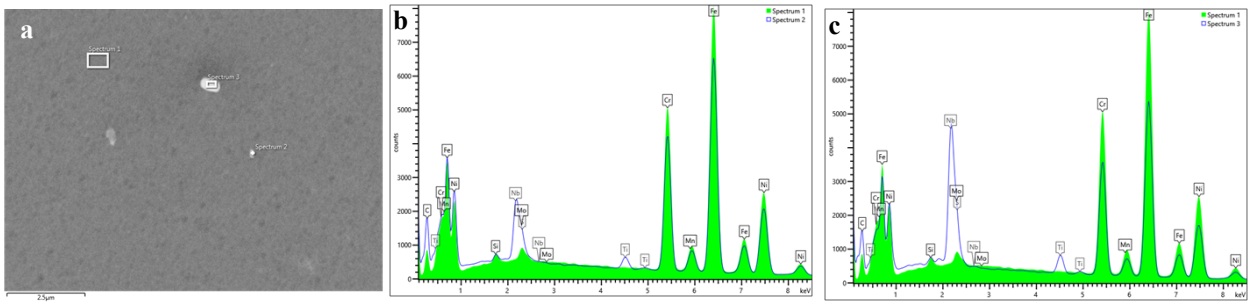

Figure 28. **(a) SE image and (b)-(c) SEM-EDX spectra obtained from fine submicron Nb-Ti-enriched inclusions present in the Carlson plate (heat 58776-3R) after the 3 h anneal at 1250°C followed by a water-quench. The EDX spectra spot analyses from 2 separate inclusions are shown as a blue line with the EDX spectrum obtained from the matrix (Spectrum 1) displayed as the solid green spectrum.**

3.2 GRAIN COARSENING STUDY: ATI PLATE - HEAT 529900-02

3.2.1 As-Received Microstructure

The as-received ATI heat 529900 -02 plate samples were also provided in the as-rolled condition. This material was characterized by an equiaxed, recrystallized grain structure, based on optical metallographic evaluation. Representative light optical micrographs are shown in Figure 29.

The EBSD inverse pole figure (IPF) of the as-received microstructure is presented in Figure 30. There was notable variation in grain size, ranging from approximately 20 μm up to ~160 μm. This is more clearly shown in the grain size frequency distribution presented in Figure 31 (a) and in the grain size versus area fraction data in Figure 31 (b). Although no severe 'necklacing' was observed (decoration of coarse deformed grains by very fine recrystallized grains), a slight indication of a network of finer recrystallized grains can be observed in Figure 29 (a).

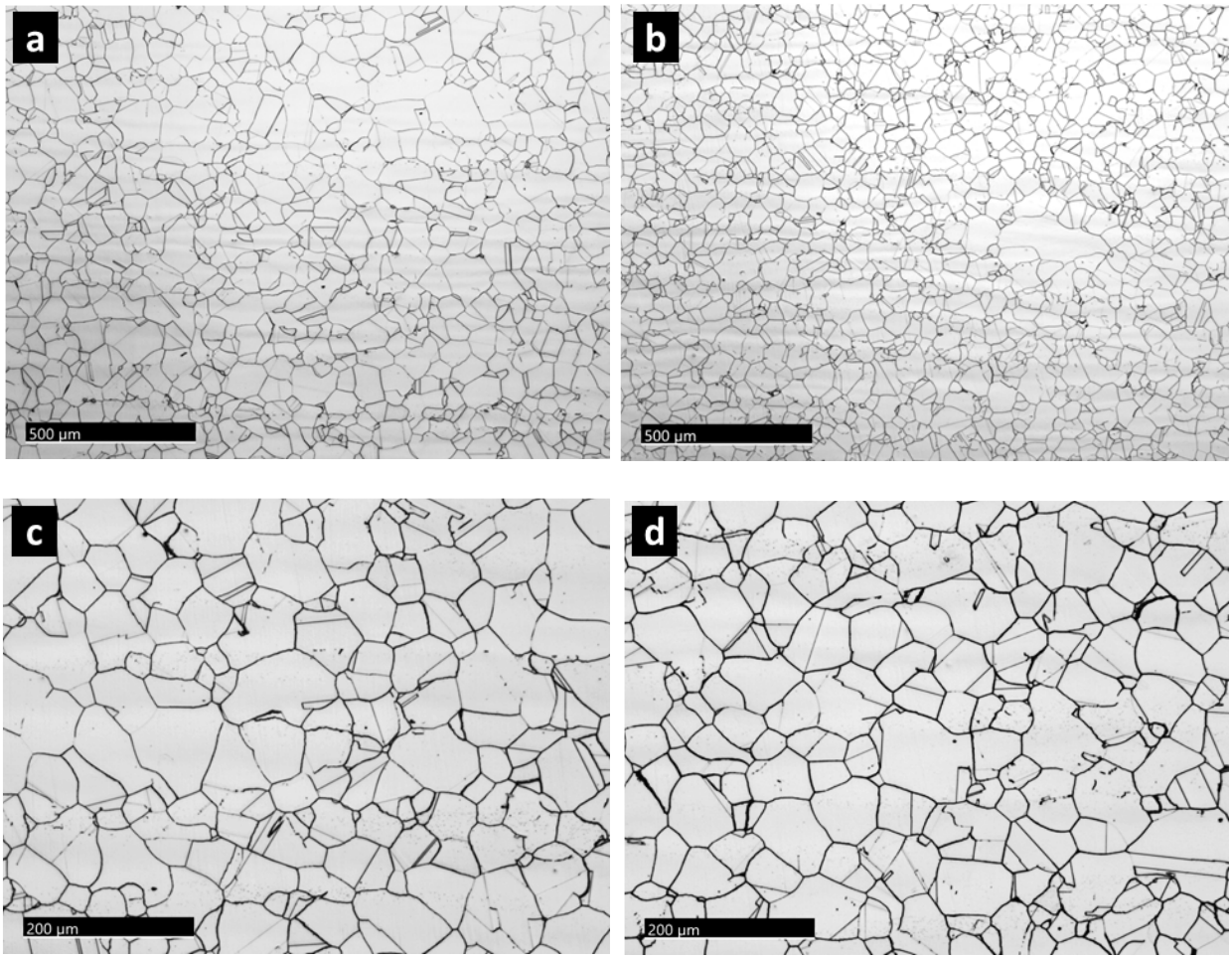

Figure 29. (a)-(d) Representative optical micrographs of the as-received ATI plate specimen.

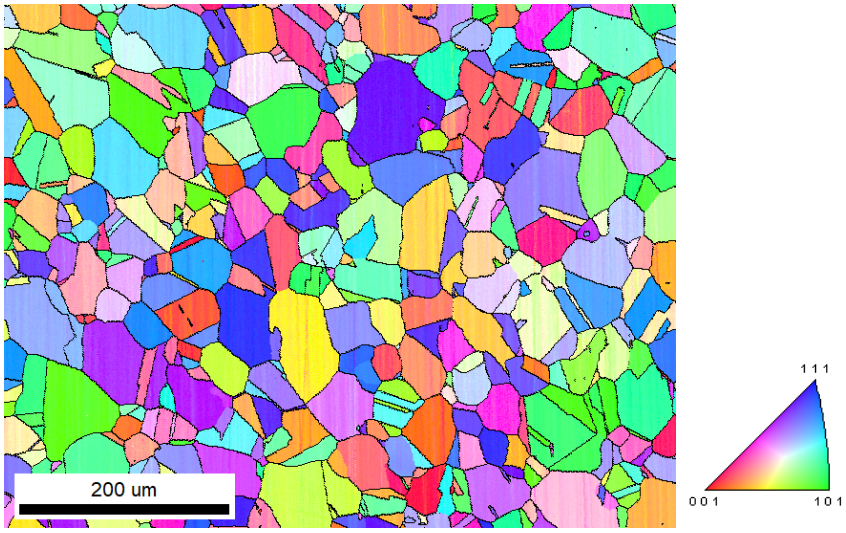

Figure 30. EBSD IPF map of the as-received ATI plate specimen.

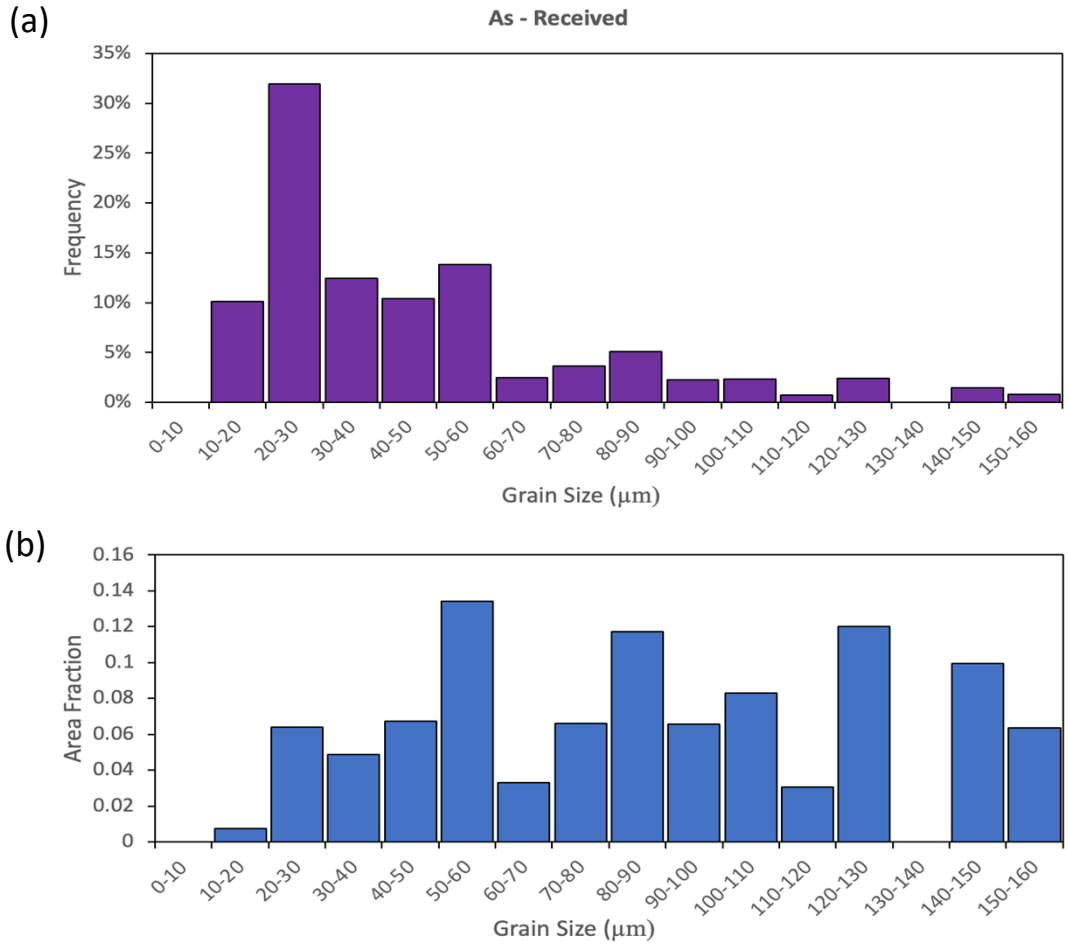

Figure 31. (a) Grain size frequency distribution and (b) grain size data plotted as a function of area fraction as measured from EBSD data obtained from the as-received ATI plate specimen.

3.2.2 As-Annealed and Water-Quenched Specimens

These as-rolled specimens were subsequently reheated at temperatures from 950 ºC to 1200 ºC for 1h followed by a water-quench (as listed in Table 2). In general, no significant localized changes were noted in terms of microstructure after the anneals at 950°C, 1000°C, 1050°C, 1100°C, and 1150°C. The results of each heat treatments on the as-received plate microstructure are presented below.

950°C/1 h: Examination of the general microstructure after the anneal at 950°C showed no major differences from the as-received plate based on optical metallography. Figure 32 provides representative light optical micrographs of the annealed plate sample. Closer examination of the microstructure revealed the presence of an apparent "ghost" structure (Figures 32 (c) and (d)) delineating some prior grains that existed earlier during the original processing of the plate. Some "bands" of darkly-imaging "particles" in Figure 32 (d) suggest some non-uniform precipitation during prior plate fabrication.

The results of the EBSD analysis are provided in Figure 33 with the IPF map for the annealed + water-quenched specimen. The grain size frequency distribution and grain size versus area fraction data generated using the OIM software are presented in Figure 34. Note that most grains analyzed were less than 20 µm in size, although grains as coarse as ~150 µm were also present.

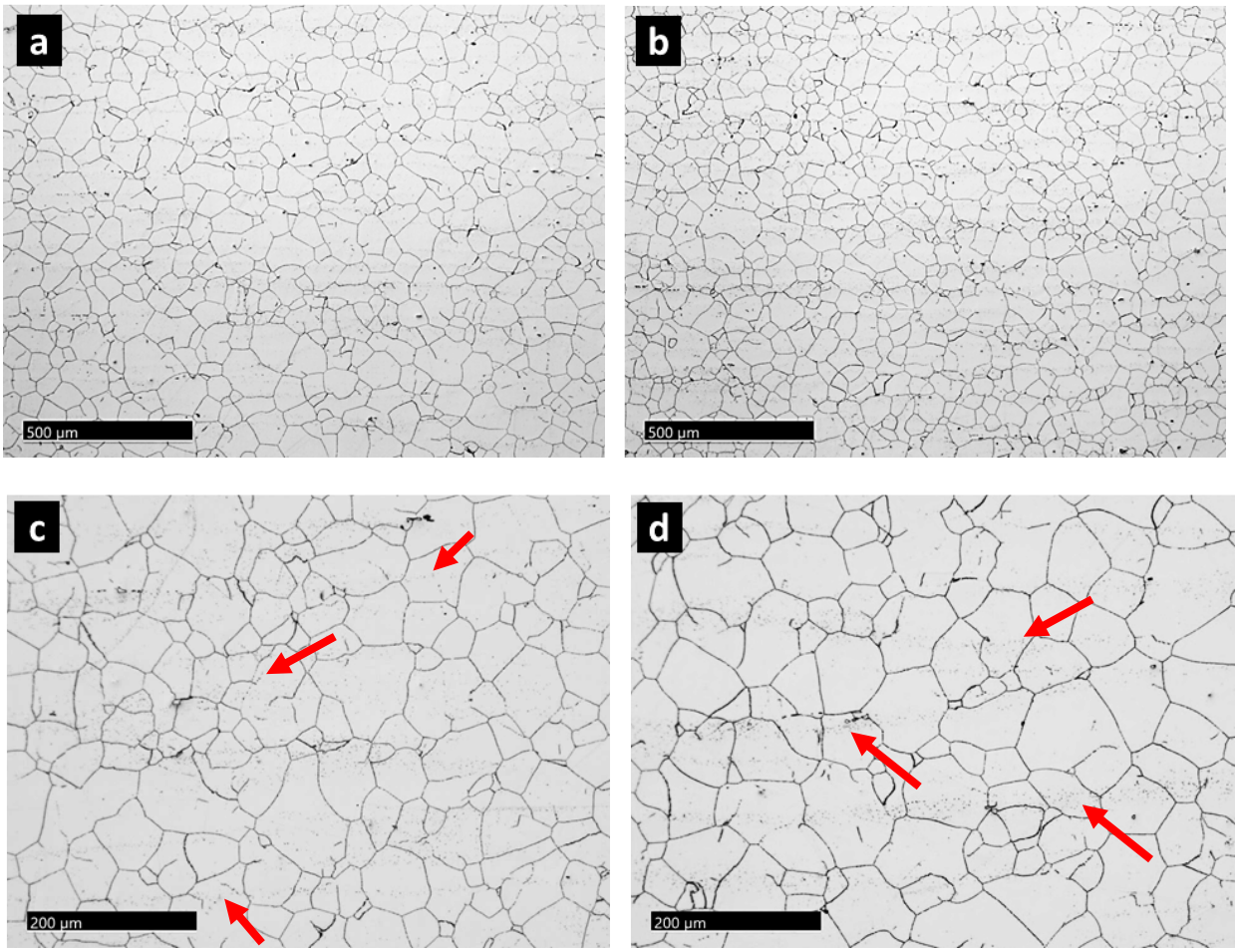

Figure 32. (a)-(d) Representative optical micrographs of the ATI plate specimen annealed at 950°C for 1 h.

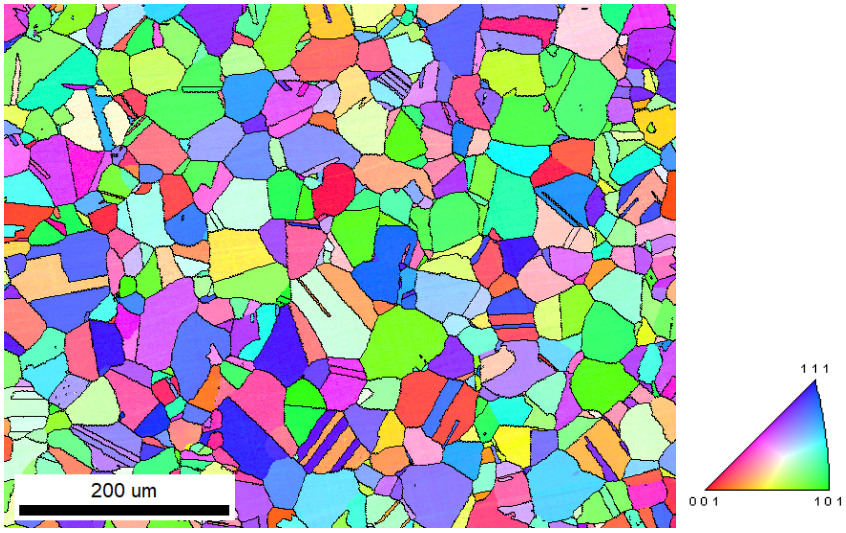

Figure 33. EBSD IPF map of the ATI plate specimen annealed at 950°C for 1 h.

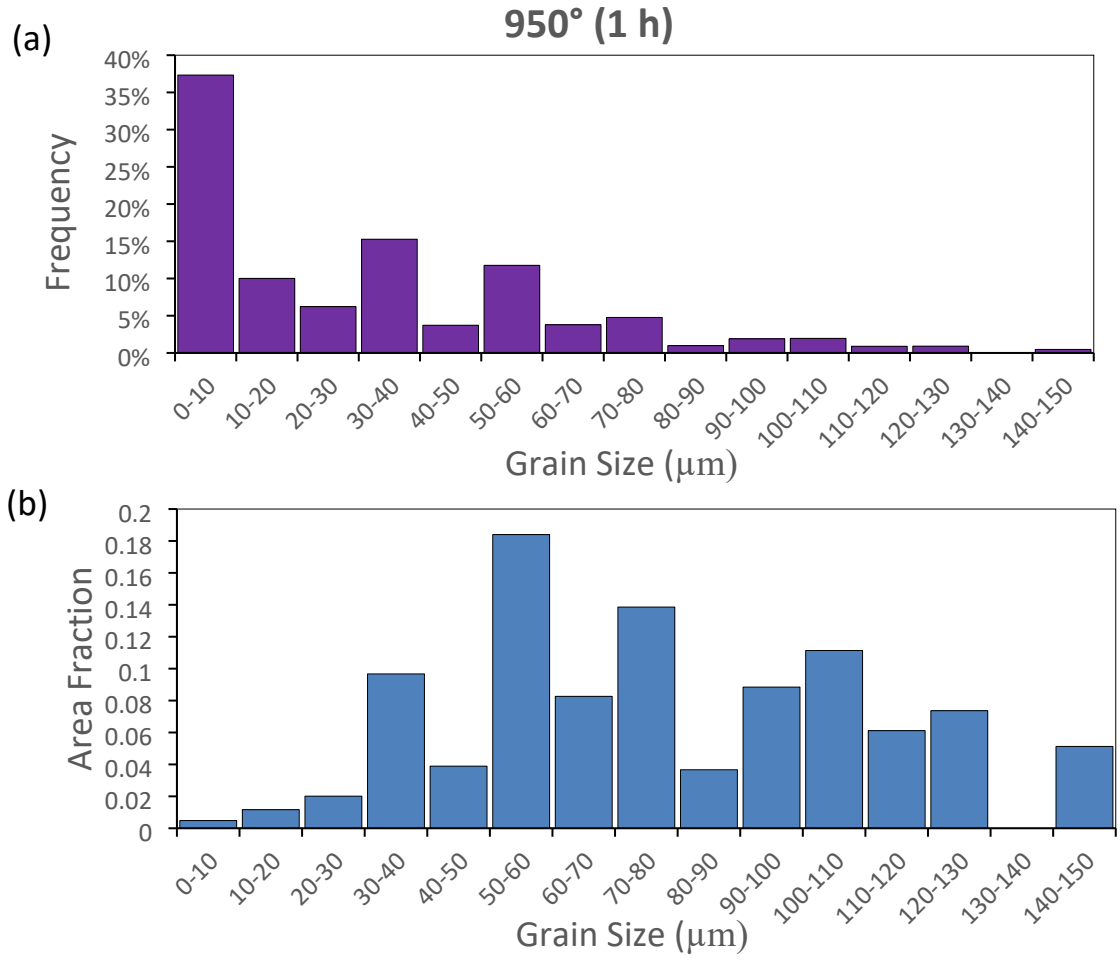

Figure 34. (a) Grain size frequency distribution and (b) grain size as a function of area fraction as measured from EBSD data obtained from the ATI plate specimen annealed at 950°C for 1 h.

1000°C/1 h: The anneal at 1000°C did not result in a significant change in microstructure from the 950°C anneal. The microstructure was characterized by the presence of equiaxed grains that ranged in size from ~20 μm to ~150 μm based on the optical micrographs of Figure 35.

EBSD data are presented in the IPF in Figure 36. The EBSD data were used to assess the grain size distribution and grain size versus area fraction, the results of which are shown in the plots in Figure 37. The majority of the grains were <~50 μm in size, with a significant portion in the 10-20 μm range. However, there was a notable presence of coarser (>100 μm) grains within the plate specimen.

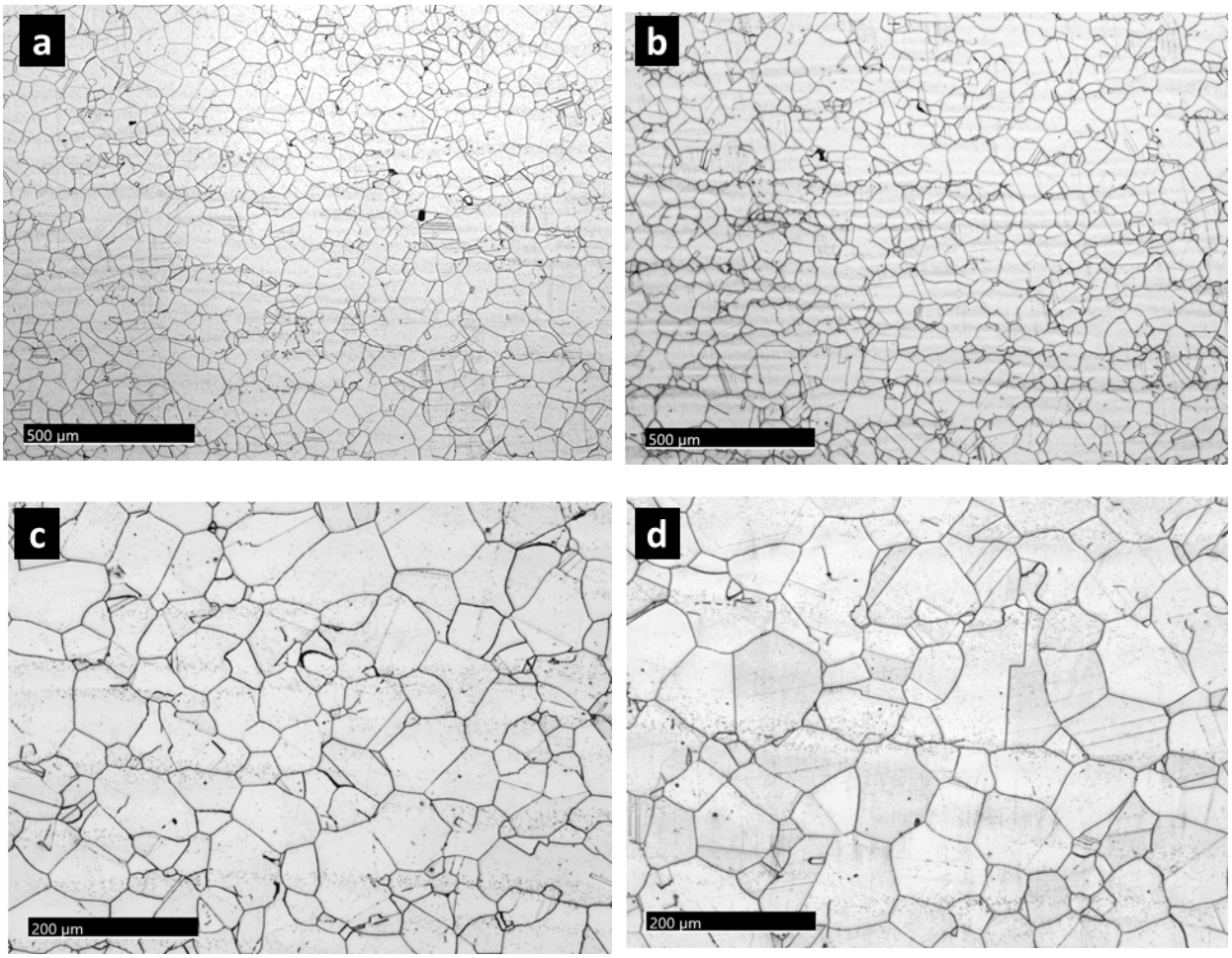

Figure 35. (a)-(d) Representative optical micrographs of the ATI plate specimen annealed at 1000°C for 1 h.

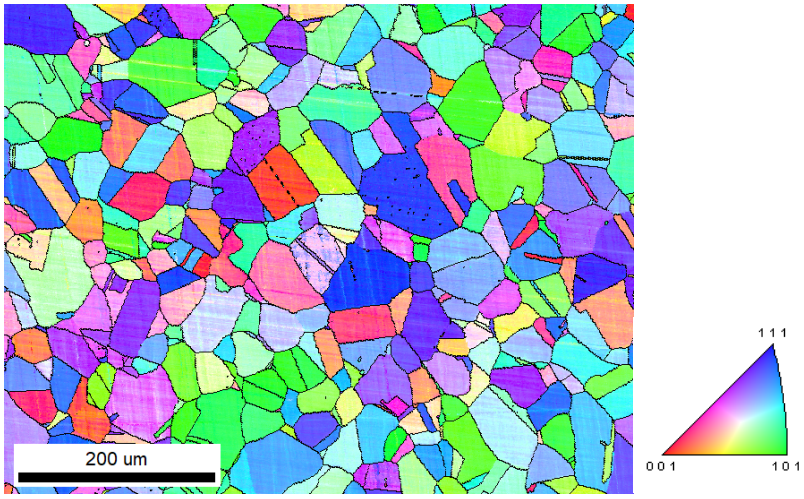

Figure 36. EBSD IPF map of the ATI plate specimen annealed at 1000°C for 1 h.

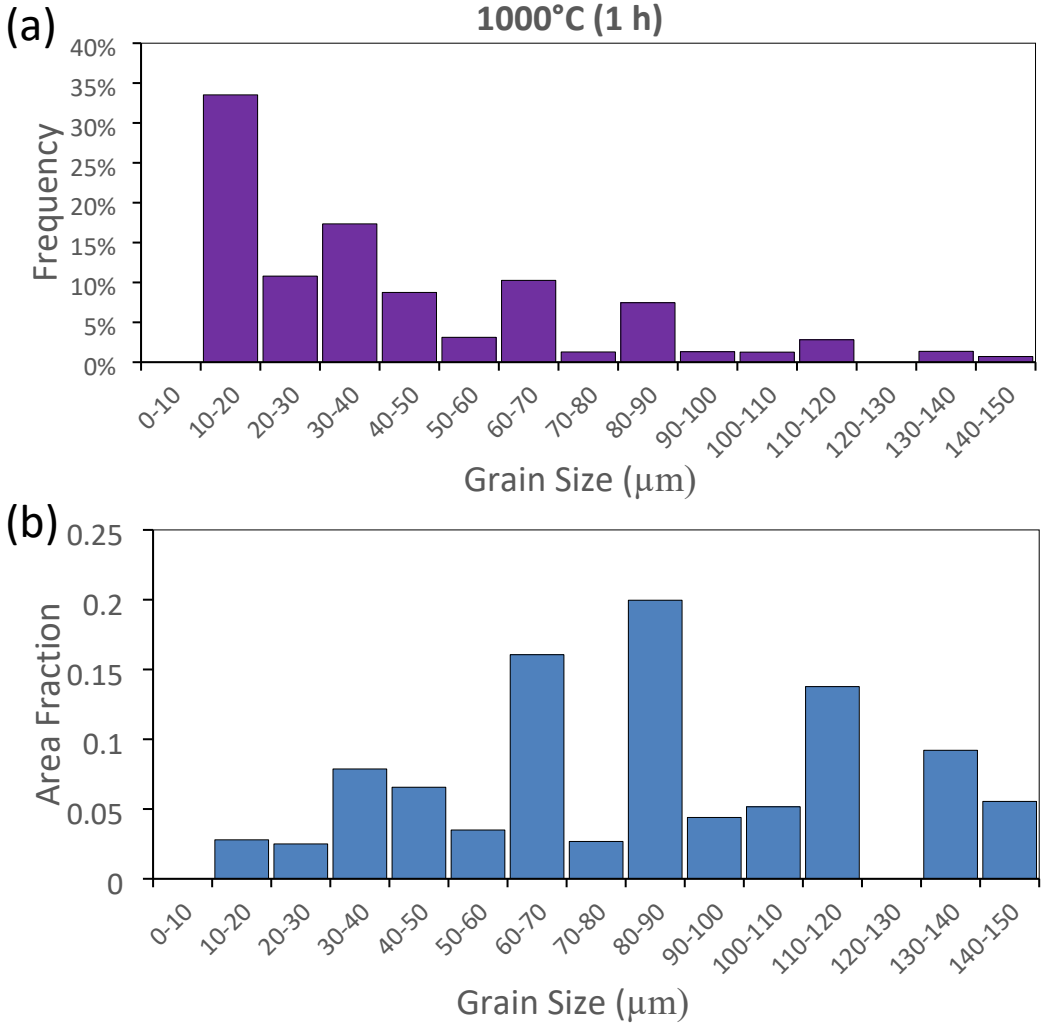

Figure 37. (a) Grain size frequency distribution and (b) grain size as a function of area fraction as measured from EBSD data obtained from the ATI plate specimen annealed at 1000°C for 1 h.

1050°C/1 h: Optical metallographic examination of the 1050°C annealed plate sample revealed a very similar equiaxed polycrystalline microstructure to those observed for the lower temperature annealing treatments. No obvious differences in grain size were noted. Discrete inclusions were observed throughout the microstructure. Representative optical micrographs are included in Figure 38.

EBSD data, presented in the IPF of Figure 39. Grain size data and area fraction data were extracted from the EBSD dataset. Figure 40 shows the grain size distribution data and the grain size versus area fraction data for the 1050°C annealed plate sample. No pronounced differences were noted between the 1050°C and 1000°C annealed specimens.

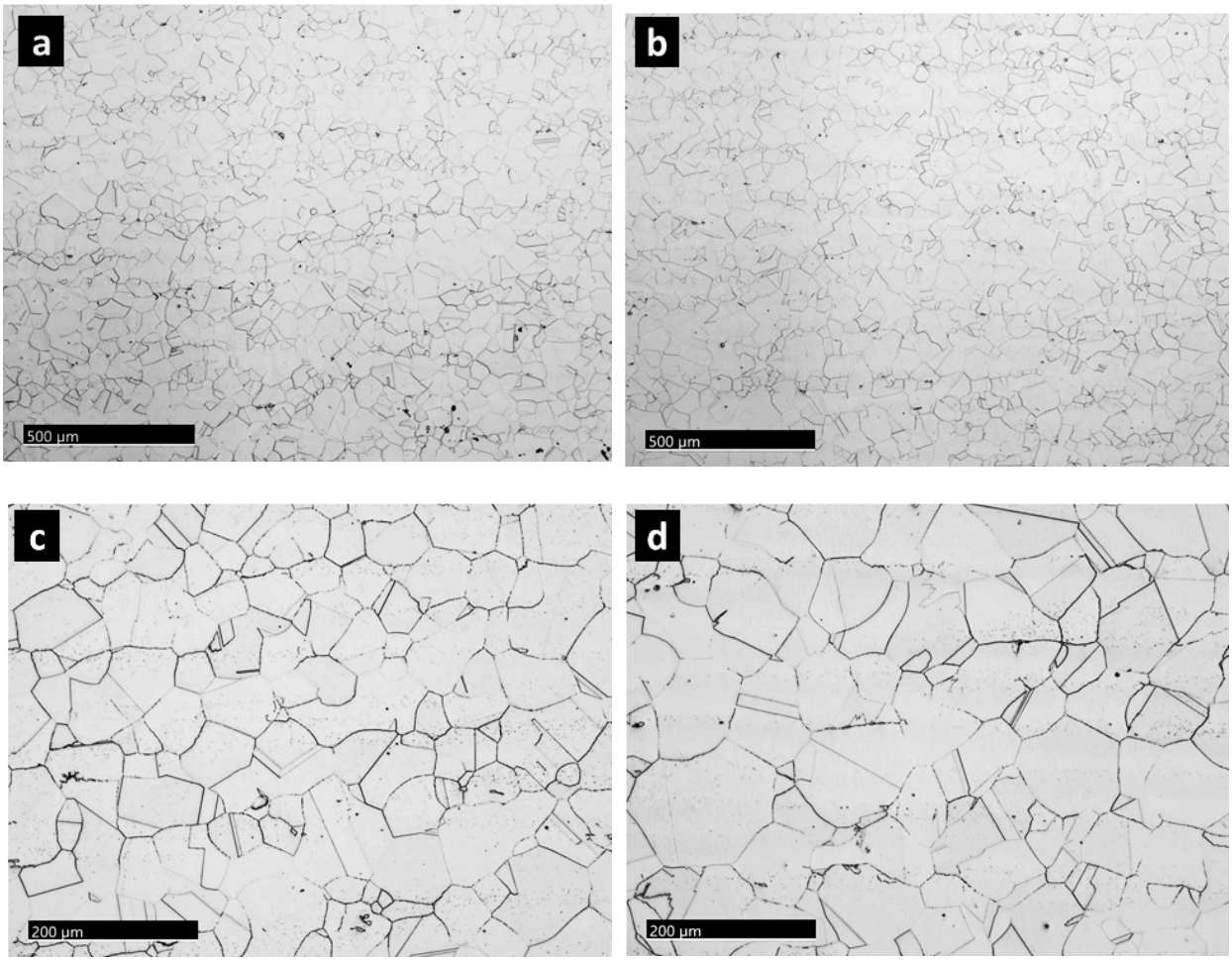

Figure 38. (a)-(d) Representative optical micrographs of the ATI plate specimen annealed at 1050°C for 1 h.

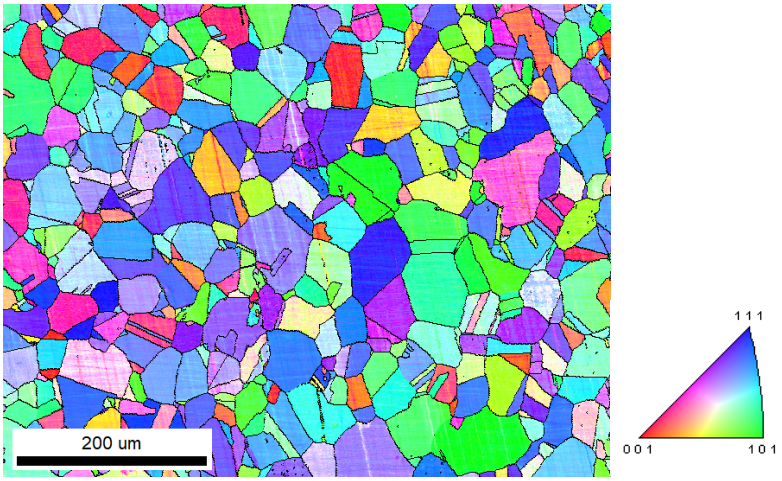

Figure 39. EBSD IPF map of the ATI plate specimen annealed at 1050°C for 1 h. Deformation associated with specimen preparation (grinding/polishing) is evident in this specimen.

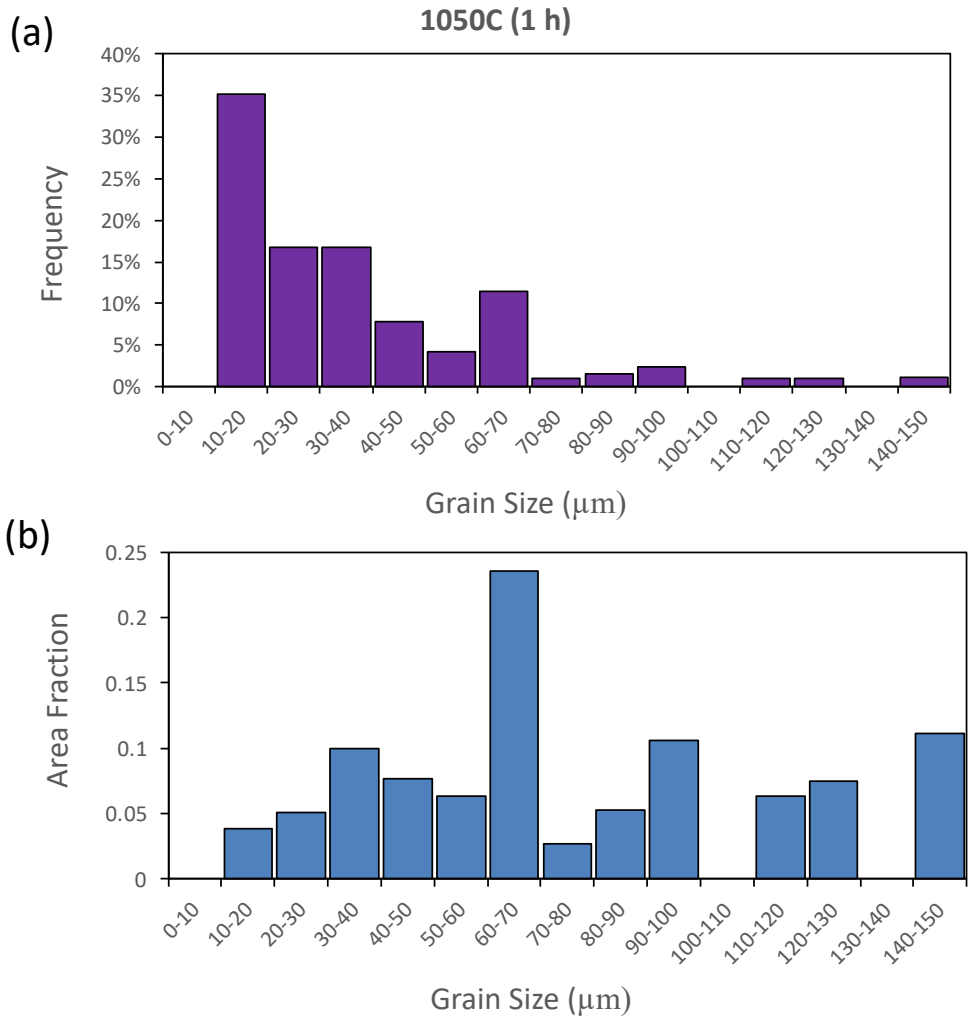

Figure 40. (a) Grain size frequency distribution and (b) grain size as a function of area fraction as measured from EBSD data obtained from the ATI plate specimen annealed at 1050°C for 1 h.

1100°C/1 h: The 1 h anneal at 1100°C resulted in some grain growth as evidenced by the optical micrographs in Figure 41. However, numerous fine grains (~20 μm), as shown in Figure 41 (d), remained in addition to the coarser recrystallized grains. More annealing twins were also observed after the 1100°C anneal.

EBSD data, presented in the IPF of Figure 42, also revealed an increased number of annealing twins compared to the specimen annealed at 1050°C. The grain size distribution and grain size versus area fraction plots also showed evidence of grain growth (Figure 43).

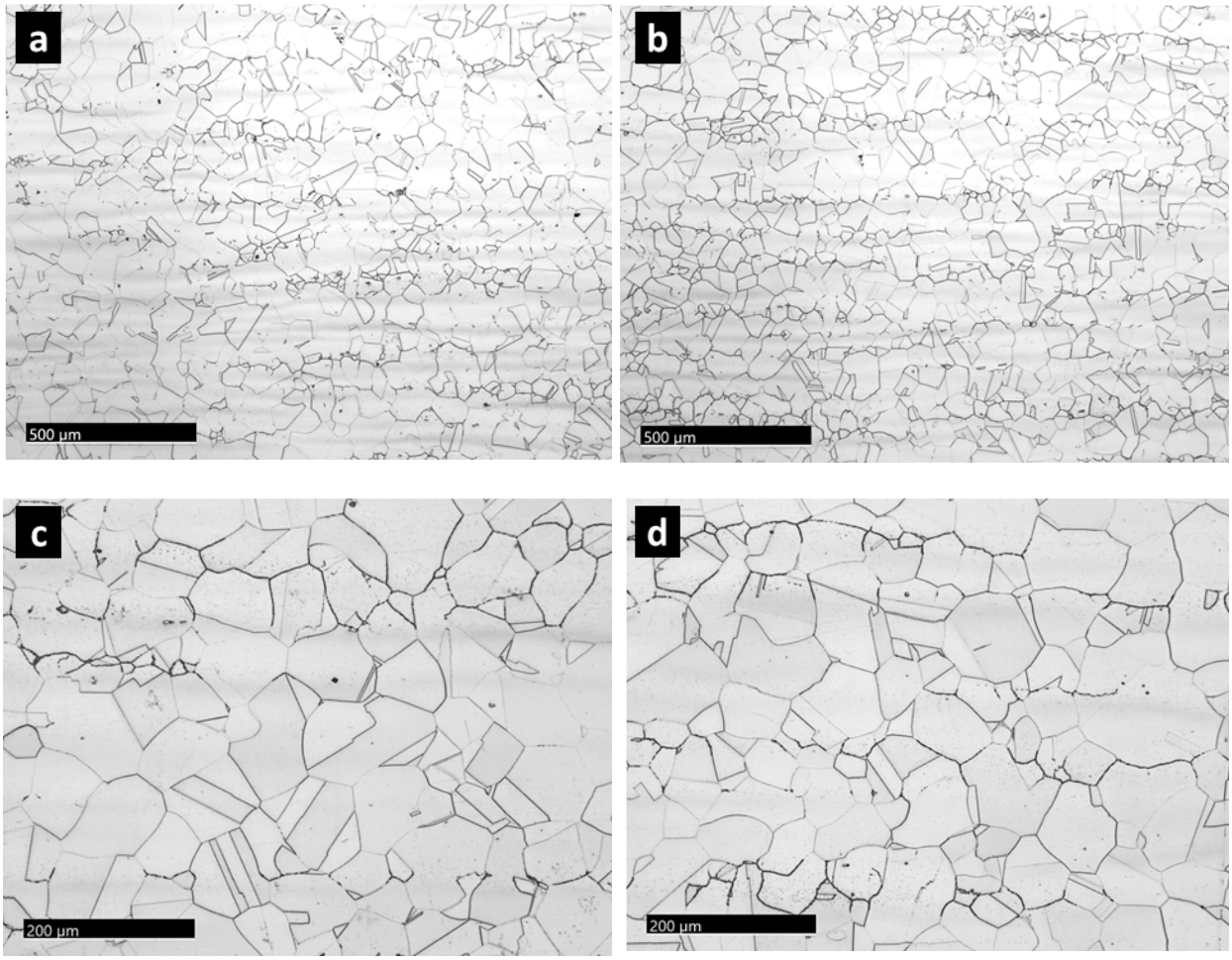

Figure 41. (a)-(d) Representative optical micrographs of the ATI plate specimen annealed at 1100°C for 1 h.

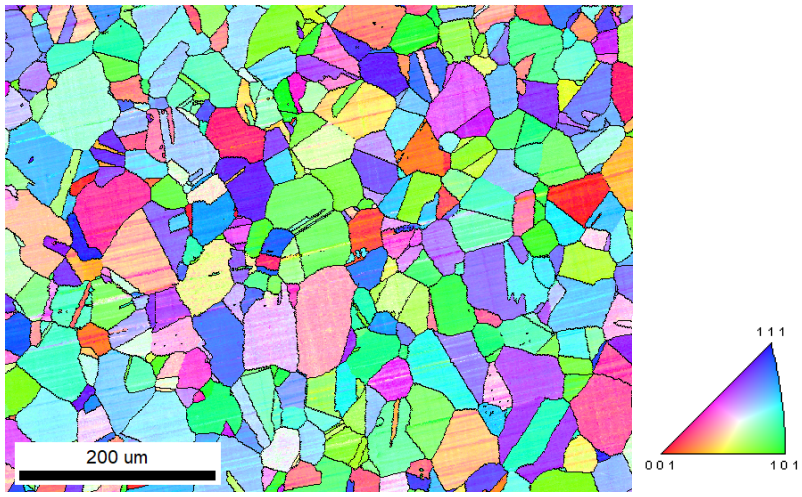

Figure 42. EBSD IPF map of the ATI plate specimen annealed at 1100°C for 1 h.

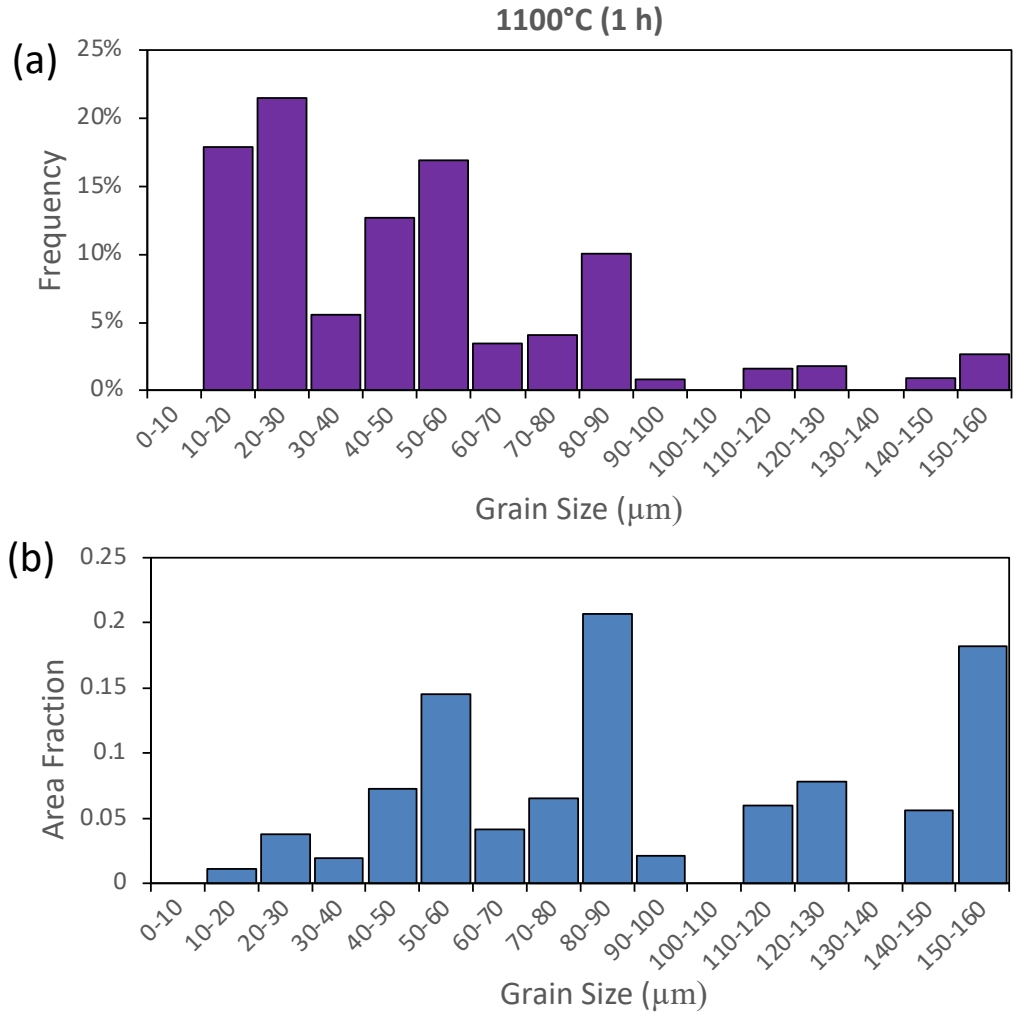

Figure 43. (a) Grain size frequency distribution and (b) grain size as a function of area fraction as measured from EBSD data obtained from the ATI plate specimen annealed at 1100°C for 1 h.

1150°C/1 h: The 1150°C anneal promoted some grain growth in the ATI plate specimen, as shown in the optical micrographs of Figure 44. The microstructure was equiaxed and moderately uniform although some isolate coarse grains were observed (Figure 44 (a)). Closer examination of the microstructure via optical metallography revealed parallel bands of very fine darkly-imaging discrete features (precipitates). Within some of these bands, discrete yellow TiN inclusions could be observed. Also, it was noted that these 'pepper'-like bands were often associated with finer grains, suggesting that these features were inhibiting grain growth.

The relative uniformity was also reflected in the EBSD data and IPF shown in Figure 45. The EBSD data were also analyzed in terms of grain size distribution and area fraction. Figure 46 includes the grain size distribution and the grain size as a function of area fraction plot, both of which show some grain growth, although fine grains are still present throughout the microstructure.

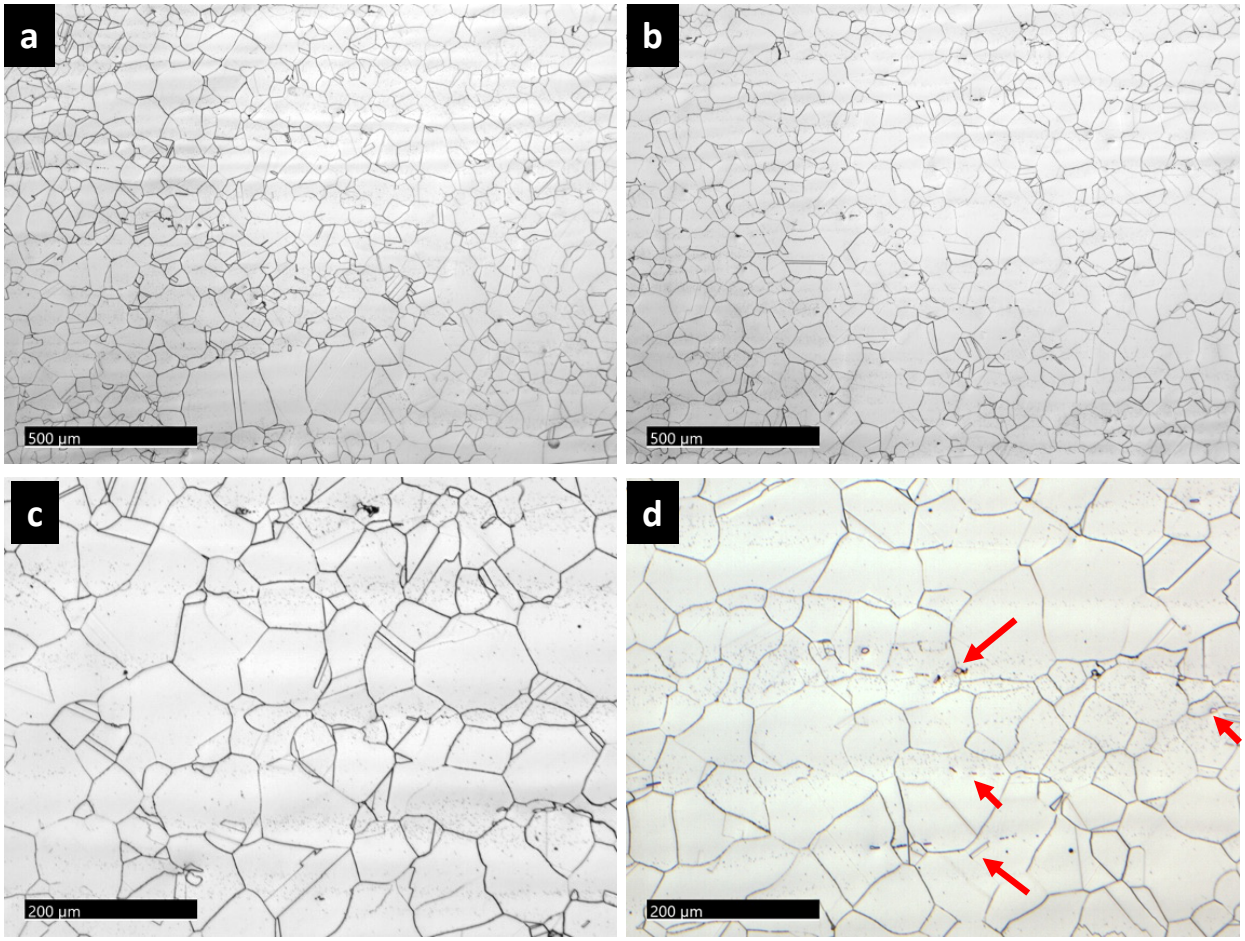

Figure 44. **(a)-(d) Representative optical micrographs of the ATI plate specimen annealed at 1150°C for 1 h. Note the variation in grain size in (a). (c)-(d) Higher magnification images showing the presence of faint 'pepper-like' contrast bands (fine precipitates) associated with the prior thermo-mechanical processing of the plate. Some yellow TiN inclusions are highlighted with red arrows. Note that some inclusions have pinned grain boundaries.**

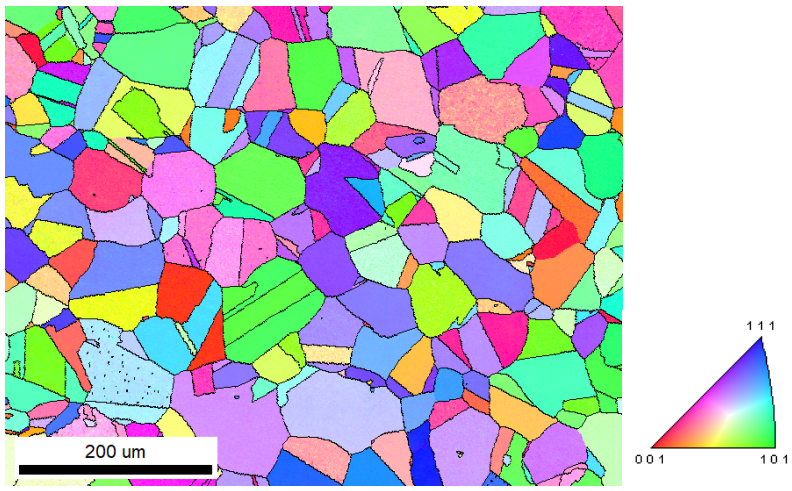

Figure 45. EBSD IPF map of the ATI plate specimen annealed at 1150°C for 1 h

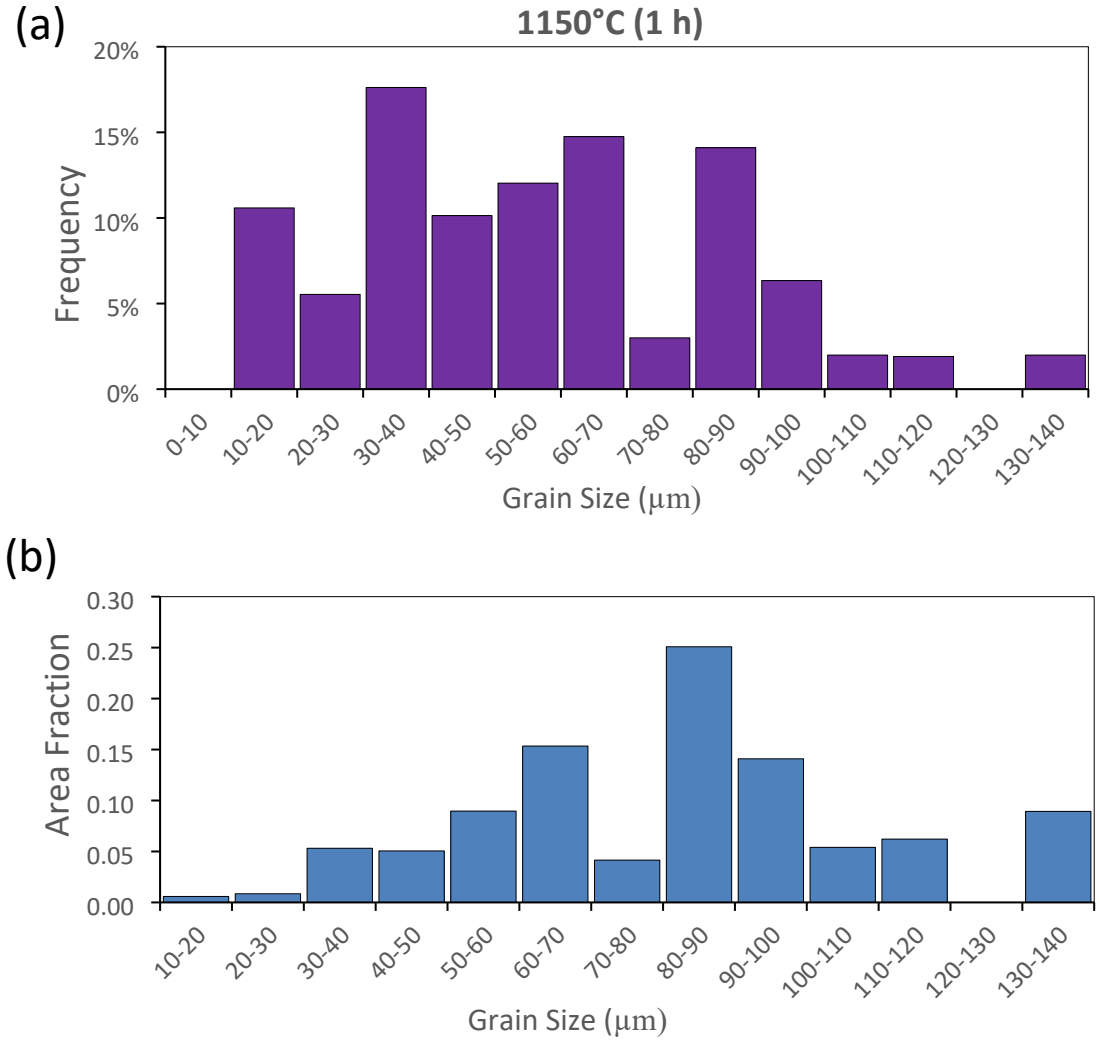

Figure 46. (a) Grain size frequency distribution and (b) grain size as a function of area fraction as measured from EBSD data obtained from the ATI plate specimen annealed at 1150°C for 1 h.

1200°C/1 h: A significant change in the microstructure was observed after the 1200°C anneal. The grain size increased dramatically, and numerous annealing twins were observed throughout the plate specimen. Some grains ~500 µm or larger were observed as well as many grains in the ~100 to 200 µm range. Representative optical micrographs are included in Figure 47. Discrete inclusions were also present throughout the specimen, some of which were aligned, and others pinned grain boundaries, as shown in Figure 47 (d). The "pepper-like" fine intragranular "banded" regions appeared to have been notably diminished after the 1200°C anneal.

The EBSD data are included in the IPF shown in Figure 48. The results of the grain size analyses are presented in Figure 49. The grain size distribution showed very significant grain growth, as did the grain size as a function of area fraction plot.

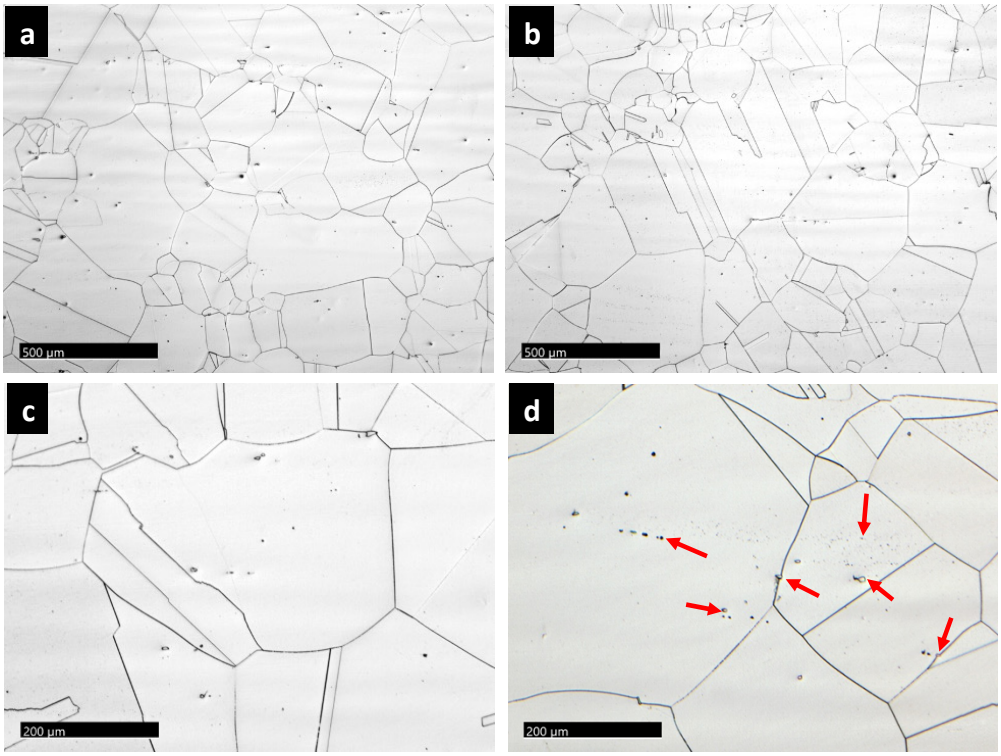

Figure 47. (a)-(d) Representative optical micrographs of the ATI plate specimen annealed at 1200°C for 1 h. Examples of the golden TiN inclusions, some pinning grain boundaries, and discrete aligned inclusions, and a region of "pepper-like" very fine inclusions are highlighted by red arrows.

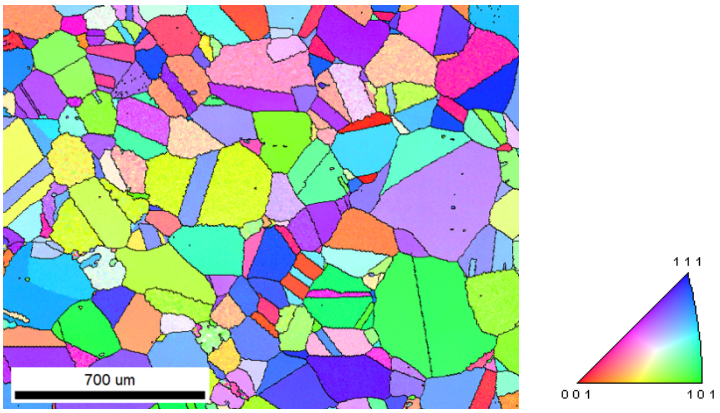

Figure 48. EBSD IPF map of the ATI plate specimen annealed at 1200°C for 1 h.

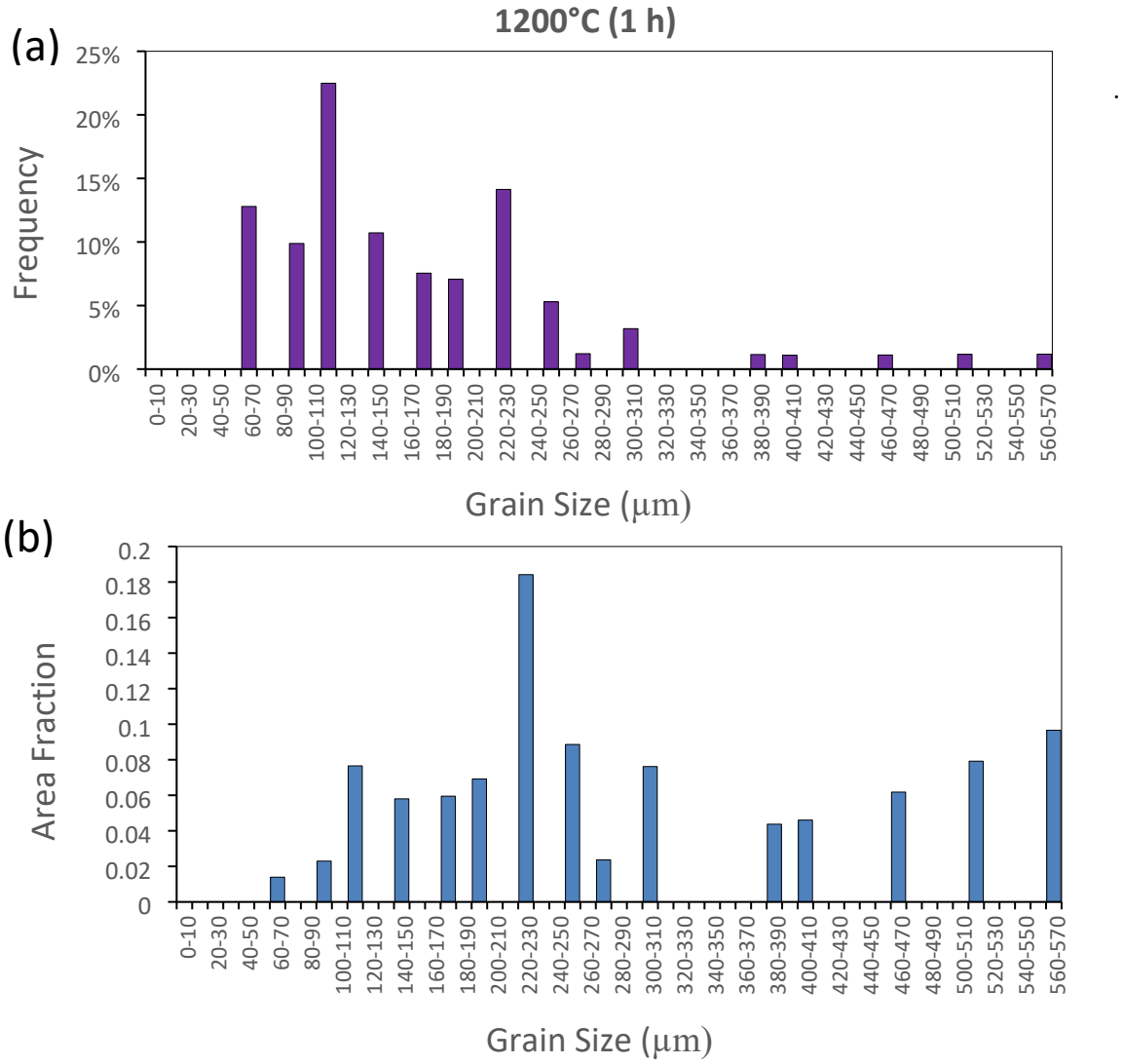

Figure 49. (a) Grain size frequency distribution and (b) grain size as a function of area fraction as measured from EBSD data obtained from the ATI plate specimen annealed at 1200°C for 1 h.

General: The grain coarsening behavior for the ATI heat 529900 -02 with the results from OM analysis and EBSD analysis for various reheating conditions is summarized in Figure 50. Examination of the average grain size as a function of annealing temperature (Figure 50 (a)) showed that the average grain size remained relatively constant at ~100 μm, with only a minor increase (to 120 μm) after the 1100°C anneal. The average grain size then increased to ~150 μm for the plate sample annealed at 1150°C. Pronounced grain growth occurred in the specimen annealed at 1200°C, with an average grain size increasing to ~325 μm. The results confirmed that grain coarsening occurred at 1200°C for ATI as-received plate. Examination of the cumulative area fraction versus grain size plot (Figure 50 (b)) confirmed the similar behavior in terms of grain size as a function of annealing temperature. The

dramatic change observed between the 1150°C and 1200°C anneals was consistent with precipitate dissolution coupled with grain growth.

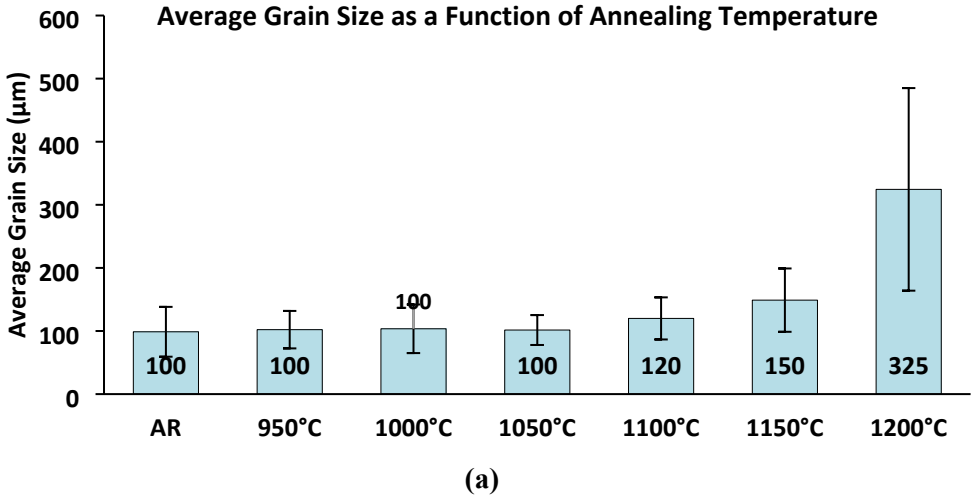

(a)

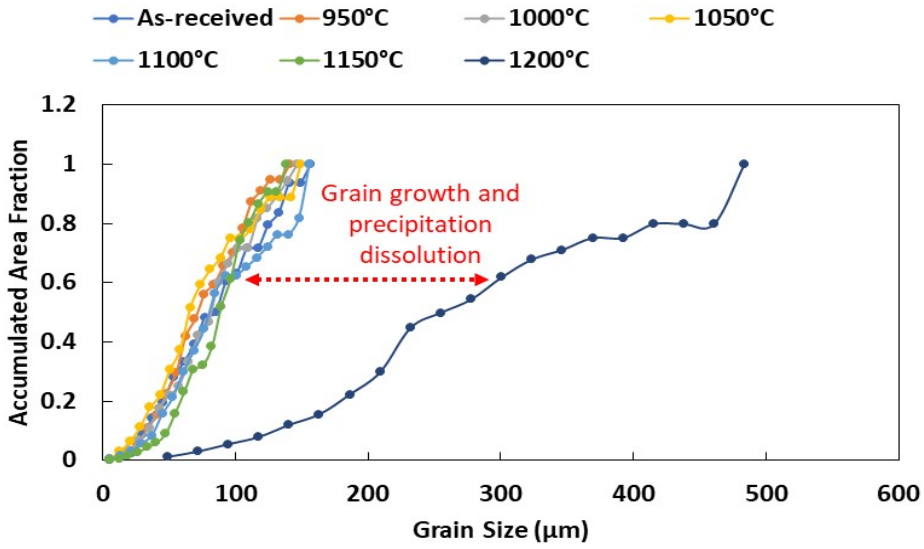

(b)

Figure 50. Summary of grain coarsening behavior for the ATI Heat 529900 -02 plate with the results from (a) OM analysis, and (b) EBSD analysis for various annealing conditions.

3.2.3 Preliminary FEG-SEM-EDXS evaluation of ATI Heat 529900-02 plate samples

A limited SEM-EDXS examination of the heavily etched metallographic specimens was performed to obtain a qualitative assessment of second-phase/precipitate dissolution during the 1 h anneal treatments. Figure 51 contains representatives SE image acquired from each annealed specimen. Brightly-imaging precipitates (assumed to be carbides or nitrides in these etched samples) were present on all grain boundaries examined for the as-received sample as well as for the samples annealed at 950°C to 1100°C. The specimen annealed at 1150°C appeared to exhibit fewer precipitates, but numerous fine 'holes' were visible, indicating that there may have been precipitate 'drop out' during the over-etching/rinsing process. The sample annealed at 1200°C contained undissolved submicron and micron-sized inclusions, with very few intergranular precipitates/carbides. It was noted that all samples contained inclusions.

The ATI as-received sample was characterized by the presence of intergranular Cr-enriched precipitates (assumed to be carbides) and Nb-enriched precipitates/inclusions throughout the microstructure. The majority of the intergranular particles were complex Cr-Nb-Mo-enriched precipitates, which started to dissolve at ~ 1150°C. After the anneal at 1200°C for 1h, it was not possible to observe intergranular precipitates, but Nb-enriched submicron inclusions remained in the matrix and occasionally were observed at grain boundaries, as shown in Figure 52.

These preliminary data provided qualitative support for the carbide dissolution at 1200°C, although further characterization via analytical electron microscopy is required.

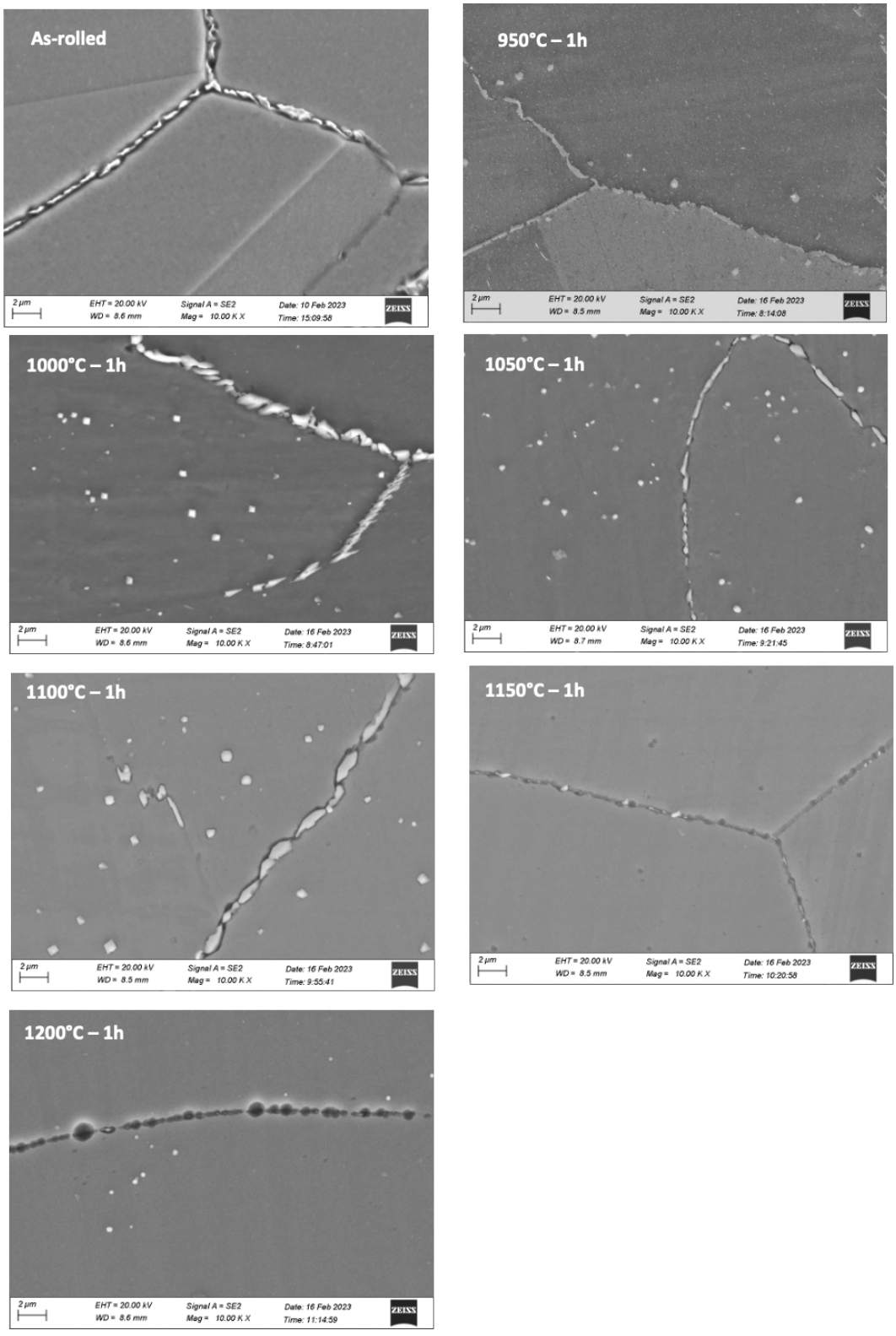

Figure 51. SE micrographs of the annealed ATI heat 529900 -02 etched plate samples. The precipitates and inclusions are brightly-imaging in these images. Note that the SE image for the etched 1150°C annealed specimen shows a series of 'holes' along the grain boundaries, which indicates that the existing precipitates were either dissolved by the etchant or 'fell out' due to over-etching.

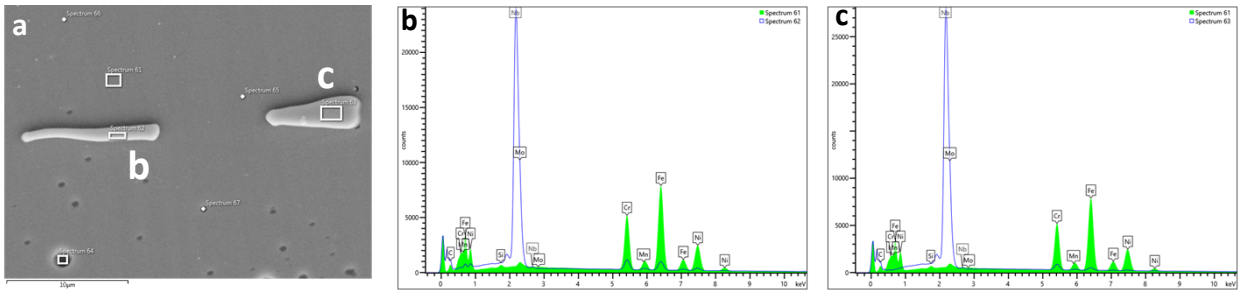

Figure 52. **(a) SE image and (b)-(c) corresponding EDX spectra from intragranular Nb-rich inclusions present in the ATI plate sample (heat 529900 -02) after the 1200°C anneal for 1 h. The green spectrum in (b) and (c) is from the matrix whereas the blue line spectrum in (b) and (c) was obtained from the inclusions labelled "b" and "c", respectively.**

4. SUMARY

The grain coarsening behavior was studied in the temperature range of 1000°C and 1250°C for the Carlson heat 58776-3R plate samples whereas the temperature range studied for the ATI heat 529900 -02 samples was 950°C to 1200°C. The two A709 as-received steel plates were under as-rolled condition. The two A709 plates exhibited different responses to the annealing treatments, consistent with the significantly different initial (as-received) microstructures. The results of this grain coarsening temperature determination study reflected the significantly different thermo-mechanical processing experienced by the Carlson and ATI A709 plates, as evidenced by the as-received microstructures of the two plates. The as-received Carlson plate was characterized by the presence of deformed, elongated grains, surrounded by very fine recrystallized grains in a "necklace"-type distribution. Such a non-uniform as-received microstructure led to the development of a non-uniform recrystallized microstructure during annealing at elevated temperatures. In contrast, the ATI A709 plate exhibited a relatively uniform, equiaxed recrystallized grain structure in the as-received (as-rolled) condition and maintained a relatively uniform grain structure as the grains grew during the elevated temperature anneals.

From this project, the following conclusion can be drawn:

1) The grain coarsening temperature, T_{GC}, for the Carlson plate (Heat 58776-3RB) was experimentally determined to be 1250°C whereas the T_{GC} for the ATI plate (Heat 529900 -02) was experimentally determined to be 1200°C.

2) An inhomogeneous as-received plate microstructure cannot be fully eliminated by high temperature anneals but was reduced although it did persist through subsequent heat treatments.

3) The use of grain size distributions to assess the microstructure should be used as opposed to the "average grain size" due to the significant inhomogeneity that can exist due to prior thermomechanical processing of plates.

Limited SEM-EDX spectrum imaging analysis provided qualitative evaluation the complex multi-phase inclusions that are typical in high N alloys, and a qualitative assessment of second phase precipitates in the steels. However, the identification of the carbides and nitrides present in the as-received and as-annealed + water-quenched conditions requires detailed Transmission Electron Microscopy

characterization, including electron diffraction data, to document the extent of nitride and/or carbonitride or carbide precipitation during the water quench from annealing temperatures. The results generated in this study will be applied to develop the continuous cooling precipitation diagrams for both the Carlson and ATI A709 steels.

REFERENCES

ASME SA-213 (2021a), Standard Specification for Seamless Ferritic and Austenitic Alloy-Steel Boiler, Superheater, and Heat-Exchanger Tubes, ASME Coiler and Pressure Vessel Code, Section II Materials, American Society of Mechanical Engineers, New York, NY (2021 Edition).

ASME (2021b), Boiler and Pressure Vessel Code, Section III Division 5, Rules for Construction of Nuclear Facility Components, American Society of Mechanical Engineers, New York, NY (2021 Edition).

T.-L. Sham, Y. Wang, R. Bass, X. Zhang (2022), A709 Qualification Plan Update and Mechanical Properties Data Assessment, INL/RPT-22-67641, Idaho National Laboratory, Idaho Falls, ID.

R. Wang, C.I. Garcia, M. Hua, K. Cho, H. Zhang, and A.J. DeArdo, "Microstructure and Precipitation Behavior of Nb, Ti Complex Microalloyed Steel Produced by Compact Strip Processing," ISIJ International 2006, 46, 1345-1353.

E.J. Palmiere, C.I. Garcia, and A.J. DeArdo, "The influence of niobium supersaturation in austenite on the static recrystallization behavior of low carbon microalloyed steels," Metallurgical and Materials Transactions A 1996, 27, 951-960, doi:10.1007/bf02649763.

Y. Wang, P.de Souza Ciacco, R. Ordonez, and C.I. Garcia, "A Comparison Study of the Austenite Grain Growth and Its Transformation Behavior during Uniform Continuous Cooling of a Wrought and Selective Laser Melting 4340Steel" Materials Performance and Characterization, 10 (2021) (ASTM) https://doi.org/10.1520/MPC20200121 <https://www.astm.org/DIGITAL_LIBRARY/JOURNALS/MPC/PAGES/MPC20200121.htm>

G. Solis-Bravo, M. Merwin, and C.I. Garcia, "Impact of Precipitate Morphology on the Dissolution and Grain-Coarsening Behavior of a Ti-Nb Microalloyed Linepipe Steel" Metals, 10 (2020) https://doi.org/10.3390/met10010089